JACS
JOURNAL OF THE AMERICAN CHEMICAL SOCIETY
Article
pubs.acs.org/JACS

Structure of Chemisorbed CO_2 Species in Amine-Functionalized Mesoporous Silicas Studied by Solid-State NMR and Computer Modeling

Luís Mafra,*[,†] Tomaž Čendak,[†] Sarah Schneider,[†] Paul V. Wiper,[†] João Pires,[‡] José R. B. Gomes,[†] and Moisés L. Pinto*[,§]

[†]CICECO - Aveiro Institute of Materials, Department of Chemistry, University of Aveiro, Campus Universitário de Santiago, 3810-193 Aveiro, Portugal

[‡]Centro de Química e Bioquímica, Faculdade de Ciências, Universidade de Lisboa, 1749-016 Lisboa, Portugal

[§]CERENA, Departamento de Engenharia Química, Instituto Superior Técnico, Universidade de Lisboa, Av. Rovisco Pais, no. 1, 1049-001 Lisboa, Portugal

Supporting Information

ABSTRACT: Two-dimensional (2D) solid-state nuclear magnetic resonance (SSNMR) experiments on samples loaded with ^{13}C-labeled CO_2, *"under controlled partial pressures"*, have been performed in this work, revealing unprecedented structural details about the formation of CO_2 adducts from its reaction with various amine-functionalized SBA-15 containing amines having distinct steric hindrances (e.g., primary, secondary) and similar loadings. Three *chemisorbed* CO_2 species were identified by NMR from distinct carbonyl environments resonating at $\delta_C \approx 153$, 160, and 164 ppm. The newly reported chemisorbed CO_2 species at $\delta_C \approx 153$ ppm was found to be extremely moisture dependent. A comprehensive ^{1}H-based SSNMR study [1D ^{1}H and 2D ^{1}H−X heteronuclear correlation (HETCOR, X = ^{13}C, ^{29}Si) experiments] was performed on samples subjected to different treatments. It was found that all chemisorbed CO_2 species are involved in hydrogen bonds (HBs) with either surface silanols or neighboring alkylamines. ^{1}H chemical shifts up to 11.8 ppm revealed that certain chemisorbed CO_2 species are engaged in very strong HBs. We effectively demonstrate that NMR may help in discriminating among free and hydrogen-bonded functional groups. ^{13}C{^{14}N} dipolar-recoupling NMR showed that the formation of carbonate or bicarbonate is excluded. Density functional theory calculations on models of alkylamines grafted into the silica surface assisted the ^{1}H/^{13}C assignments and validated various HB arrangements that may occur upon formation of carbamic acid. This work extends the understanding of the chemisorbed CO_2 structures that are formed upon bonding of CO_2 with surface amines and readily released from the surface by pressure swing.

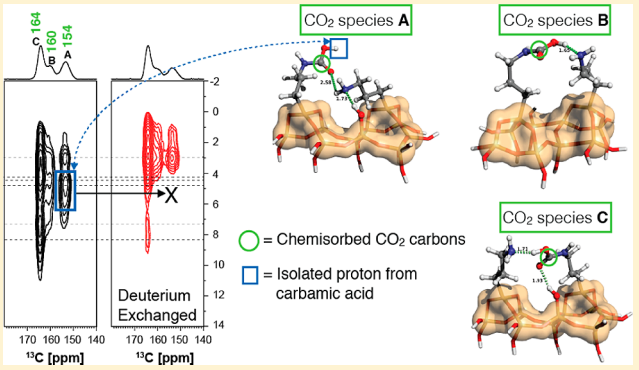

1. INTRODUCTION

In the struggle to reduce CO_2 concentrations in the Earth's atmosphere to prevent an increase in the greenhouse effects, the scrubbing of flue gases from stationary sources is assuming a critical role. In recent years, several adsorbent materials have been studied for the selective adsorption/capture of CO_2 in order to substitute the classical scrubbing of gases with aqueous amine solutions. Absorption with these solutions poses several disadvantages, including corrosion problems and the low energy efficiency due to the high temperatures used in the regeneration step. Among the materials that are being developed, amine-functionalized porous sorbents are the most significant ones[1,2] as they have high selectivity and capacity toward CO_2 at low partial pressures even in the presence of moisture.[3−8] This is an advantageous feature for post-combustion gas capture applications where CO_2 exists at relatively low concentrations.[9] Usually, mesoporous silicas, such as SBA-15, used in this work, are widely used to introduce high amounts of covalently tethered amines (typically above 2 mmol g^{-1}, up to 4−5.8 mmol g^{-1})[10,11] since they are very stable and have pores that can facilitate the functionalization process.[2] Although high production cost and difficulties at scale-up may impair certain future large-scale applications of these materials, the high selectivity and energetic efficiency make them very attractive for some industrial applications, including air purification by selective extraction of CO_2.[12]

There are two main functionalization strategies that have been studied and are reported in the literature. The first one consists of impregnating the porous support with amine rich polymers or promoting the polymerization of such polymers inside the pores. In this case, the porous material can be

Received: October 24, 2016
Published: December 13, 2016

DOI: 10.1021/jacs.6b11081
J. Am. Chem. Soc. 2017, 139, 389−408

regarded as a molecular basket for the polymer.[13] The main disadvantages of this process are a significant reduction in the pore volume and accessibility, adversely affecting the adsorption kinetics. The second strategy is the grafting of amine functional groups on the surface of the silica pores, usually using alkoxysilane amines.[14] This leads to materials with higher porous volumes and accessibility than materials impregnated with polymers, although the number of amine functional groups is typically lower.

A large number of articles about CO_2 adsorption on porous amine-functionalized mesoporous silica (AFMS) sorbents were published already, with most focusing on the development of materials with higher CO_2 adsorption capacity and on the optimization of the synthesis procedure.[1,2,15−17] Since the first publications, the mechanism for the retention of CO_2 by the amines in AFMS is assumed to be essentially the same as in aqueous amine solutions.[14] Namely, it is assumed that CO_2 reacts with two amines to form an alkylammonium carbamate ion pair. In the present work we will show that this assumption is not correct for all chemisorbed CO_2 species and that the chemical nature of the silica substrate strongly influences the species that are formed. Furthermore, studies focused on the atomic-level understanding of chemisorbed CO_2 species formed at the pore cavities are still scarce, with most investigating the molecular basis of the adsorption mechanism derived primarily from infrared (IR) spectroscopy.[10,13,14,18−23] However, the analysis of IR spectra represents several difficulties in the assignment of the vibrational bands because silica is not transparent to IR and it holds also intrinsic strong broad bands that overlap significantly the bands due to the grafted organic groups and the chemisorbed species, often leading to disagreements with respect to the band assignments in the literature.[1,2]

Solid-state nuclear magnetic resonance (SSNMR) is a powerful alternative, which is able to selectively study the local intermolecular interactions and to discriminate between similar chemical species. Existent SSNMR caracterization studies are often used to confirm the connectivity mode of amines at the pore surface using ^{13}C and ^{29}Si MAS NMR routine measurements. However, the number of SSNMR studies on the structure of adsorbed CO_2 species in AFMS is rare and usually based solely on one-dimensional (1D) SSNMR experiments.[24,25] The existence of theoretical studies involving an in-depth study of CO_2−amine interaction in AFMS by means of molecular simulations is equaly scarce.[26]

In a previous work, we used ^{13}C SSNMR spectroscopy to confirm the formation of unstable (i.e., easily removed just by applying high vacuum without thermal treatment) carbamic acid at ca. 160 ppm and carbamate ion pairs at ca. 164 ppm in a porous material functionalized with a primary amine and loaded with isotope-enriched $^{13}CO_2$.[27] We have also studied their related temperature dependencies and confirmed their assignment by density functional theory (DFT) calculations of ^{13}C chemical shifts (CSs) using simplified molecular models. Until now, the most relevant SSNMR studies on AFMS investigated the molecular mechanism of CO_2 deactivation in supported amines under dry and humid conditions.[7,28,29] For example, Sayari et al. prepared amine-modified PE-MCM-41 and urea-grafted PE-MCM-41 materials loaded with CO_2 subjecting the materials to multiple CO_2 adsorption−desorption cycles under dry conditions and have detected a ^{13}C resonance at ca. 160 pm in both materials, which was assigned to a urea species.[7] However, under humid conditions this resonance did not appear. This result pointed toward an increased stability/durability of CO_2-loaded AFMS in moisture-containing gases as urea formation was quenched in the presence of moisture. In other fundamental studies,[28,29] it was observed that CO_2 uptake was increased with primary amines when compared to more sterically hindered amines since CO_2 reactivity critically depends on amine accessibility. In addition, the stability difference of primary, secondary, and tertiary monoamines and multiple linear and branched polyamines was associated with the formation of isocyanate intermediate species leading to the formation of undesired urea linkages. Numerous ^{13}C CPMAS NMR measurements were employed to monitor the formation of these urea derivatives formed before and after extensive CO_2 adsorption−desorption cycling, showing that the range of ^{13}C NMR CSs for C═O groups in different urea derivatives is ∼160−163 ppm.[29] This extremely narrow range renders the precise resonance assignment very difficult. Nevertheless, this reported CS range was obtained considering a molecule in the gas phase and does not take into consideration intermolecular interactions in the solid-state, which may considerably change the local chemical environment surrounding the interacting nucleus. Although building suitable models to perform calculations of atomic properties in such large systems is a challenging task, a few recent publications describe Monte Carlo molecular simulations in the study of CO_2−surface interactions in large models of AFMS at the expenses of losing the effects of the electronic structure.[30,31] However, it has been recognized that theoretical chemistry approaches in this field should be combined with experimental assessment.[32] An important example of such combination is the recent study by Hahn et al.[26] where IR spectroscopy and thermogravimetry were combined with B3LYP+TS//BLYP +TS electronic structure calculations and two different finite cluster models to analyze the role of primary, secondary, and bifunctional amines on the interaction of CO_2 with SiO_2 spheres.

To date, several aspects remain unclear, for example, the intermolecular interactions between neighboring amine groups and the role of these interactions in the stabilization of the formed species. Also, the effect of the silica substrate, namely surface silanol groups, is poorly understood although it was found that such silanol groups influence the species formed upon CO_2 adsorption and activation.[18,20,33] It was also reported that the amine surface density, which depends strongly on the host material and synthesis procedure, plays an important role in the amine···amine and amine···support interactions involved in CO_2 adsorption.[34] A detailed understanding of the adsorbate−adsorbent interactions is thus crucial to propel porous adsorbent design toward ideal CO_2 adsorption−desorption behavior. It is important to obtain a reliable molecular identification of formed species before CO_2 and oxidation-induced degradation studies can be interpreted, since molecular moieties derived from degradation of amines will strongly depend on the chemical nature of CO_2−amine adducts formed in first place. Unfortunately, a comprehensive atomistic study of CO_2−amine interactions on AFMS materials containing amines with distinct steric hindrances is still lacking. Moreover, there are still many uncertainties regarding the nature of hydrogen bonds (HBs) involving chemisorbed CO_2 species; the ability to correlate ^{1}H and ^{13}C spins through 2D NMR and access C···H proximities is therefore an extremely valuable asset that was not explored yet.

DOI: 10.1021/jacs.6b11081
J. Am. Chem. Soc. 2017, 139, 389−408

To cover this gap and shed light on the nature of chemisorbed CO_2 species formed, the present work combines a SSNMR and computational study of various amine-grafted SBA-15 materials loaded with ^{13}C-labeled CO_2 ($^{13}CO_2$) at "*variable pressures*"—from very low (0.13 kPa) to ambient (100 kPa) pressures—under tightly controlled atmosphere. This strategy overcomes the insensitivity problems inherent to the SSNMR technique by boosting the NMR signal of samples loaded with $^{13}CO_2$, enabling us to take advantage of more advanced 1D and 2D SSNMR methods to improve assignment of the local chemical environment of the formed species. To attain this goal, high-resolution 2D $^1H-^{13}C/^{29}Si$ Lee–Goldburg cross-polarization (LG-CP) heteronuclear correlation (HETCOR) experiments were employed: such NMR experiments were also employed in deuterium exchanged materials prior to $^{13}CO_2$ adsorption to aid the assignment of resonances. $^{13}C-\{^{14}N\}$ recoupling experiments were used for selective observation of nitrogen-bonded carbons, and variable contact-time CP experiments were recorded to access the dynamics and structure of grafted amines before and after $^{13}CO_2$ adsorption. Molecular models of the silica surface functionalized with amines (with and without bonded CO_2) engaged in different intermolecular interactions were studied using DFT methods, and results were compared with the experimental values to assess the accuracy of the methods and models. By combining SSNMR and computational methods with experimental IR data from the literature, the assignment of the observed NMR resonances with confidence was possible. This approach has proven efficient in identifying the formation of carbamic acid stabilized via very strong HB with lateral amines and/or silanol groups of the silica support.

One of our goals was also to study the CO_2 structure when the chemical nature of the amine is changed. Therefore, we measured the adsorption on SBA-15 materials functionalized with primary [3-aminopropyltriethoxysilane (APTES)], secondary [trimethoxy[3-(methylamino)propyl]silane (TMMAP)], and tertiary ([3-(diethylamino)propyl]trimethoxysilane (3-DEAPTES)) amines, and also in a diamine containing primary and secondary amine groups [*N*-[3-(trimethoxysilyl)propyl]-ethylenediamine (N-3)] (Scheme 1). We have, however, restricted most of our efforts to study materials modified with APTES and TMMAP as these two present significant differences in CO_2 adsorption at similar loadings while the discussion involving the other two materials was kept to the essential. This works yields a comprehensive view of the molecular complexity of the amine capturing capability. We also demonstrate by SSNMR which amine sites are populated in the first place upon CO_2 chemisorption as CO_2 partial pressure is increased. This is important because in many "real-world" CO_2 capture technologies (e.g., postcombustion CO_2 capture) partial pressures below 1 bar are typically employed; therefore, SSNMR measurements at low CO_2 partial pressure ranges are crucial for understanding CO_2–amine interactions in mesoporous silicas.

Scheme 1. Structure of the Alkoxysilanes Used in the SBA-15 Functionalization[a]

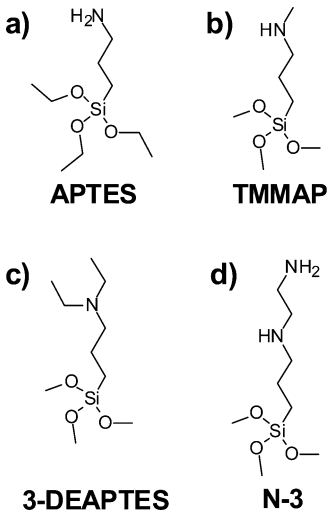

[a]See text for the full chemical name of each molecule.

2. METHODS

2.1. Materials Synthesis. The method of SBA-15 synthesis was taken from the literature.[35] According to this method about 4.0 g of copolymer (EO)20(PO)70(EO)20 (Aldrich) was dissolved in 126 cm^3 of 1.6 M HCl solution. Next, 9.1 cm^3 of tetraethyl orthosilicate (TEOS, Aldrich) was added to this solution with constant stirring. The solution was then stirred at 35 °C for 24 h and subsequently heated at 100 °C for 24 h, under static conditions. Afterward, the solution was filtered, and the obtained solid was dried in air. The solid was calcined at 550 °C for 5 h with a ramp of 1 °C/min. The resulting material (SBA-15) was stored in a desiccator for further use.

SBA-15 functionalization was prepared with amino-organosilanes; APTES (purity >98%), TMMAP (97%), N-3 (97%), and 3-DEAPTES (96%), all acquired from Sigma-Aldrich. It is worthwhile mentioning that the dryness conditions of the reaction media and material are of paramount importance to prevent extension of lateral silane polymerization within the materials and to allow an efficient silane functionalization. To achieve this, typically 2 g of SBA-15 was introduced in a closed reflux apparatus connected to a vacuum line and heated to 150 °C for 2 h. After cooling, the nitrogen was introduced into the system prior to the opening of the reflux apparatus, and SBA-15 was refluxed with 100 cm^3 of dry toluene (Aldrich, 99.8%) containing 9 mmol of the amino-organosilane for 24 h in a nitrogen atmosphere. The resulting materials with each amino-organosilane were purified by Soxhlet extraction with dry toluene, to remove the unreacted amino-organosilanes, and finally dried under vacuum, at 120 °C for 24 h. Functionalized materials were named amino-organosilane@SBA-15, where the amino-organosilane can be APTES, TMMAP, N-3, or 3-DEAPTES.

2.2. Materials Characterization. The porous texture characterization of the materials was made by N_2 adsorption at −196 °C. The N_2 adsorption isotherms were obtained in an automatic apparatus Micromeritics ASAP 2010. Before the isotherms measurement, the samples (~50 mg) were outgassed during 2.5 h at 150 °C under vacuum greater than 10^{-2} Pa. From N_2 adsorption data the specific surface area (A_{BET}) was determined through Brunauer–Emmett–Teller (BET) equation in the $0.05 < p/p^o < 0.2$ pressure range,[36] and the total pore volume (V_{total}) was assessed by the Gurvich rule,[36] corresponding to the volume of N_2 adsorbed at $p/p^o = 0.95$. The mesopore size distributions were obtained by the Broekhoff–de Boer method, in a version simplified with the Frenkel–Halsey–Hill equation[37] that was previously shown to give accurate results when applied to mesoporous silicas and silicates.[38]

Thermogravimetry with differential scanning calorimetry (TG-DSC) experiments were carried out in an apparatus (Setaram TG-DSC 111) with 0.001 mg and 0.05 mW of precision, using about 10 mg samples, between 25 and 600 °C, under dry air flux (Air Liquid). From the mass loss between 150 and 500 °C, the organic content of samples was determined. This temperature range corresponded to the exothermic peaks observed on the heat flow curves, assigned to the decomposition of the organic linkers in air.

2.3. CH_4 and CO_2 Adsorption above Atmospheric Pressure. The adsorption isotherms of CO_2 and CH_4 (Air Liquide, 99.995%)

DOI: 10.1021/jacs.6b11081
J. Am. Chem. Soc. 2017, 139, 389–408

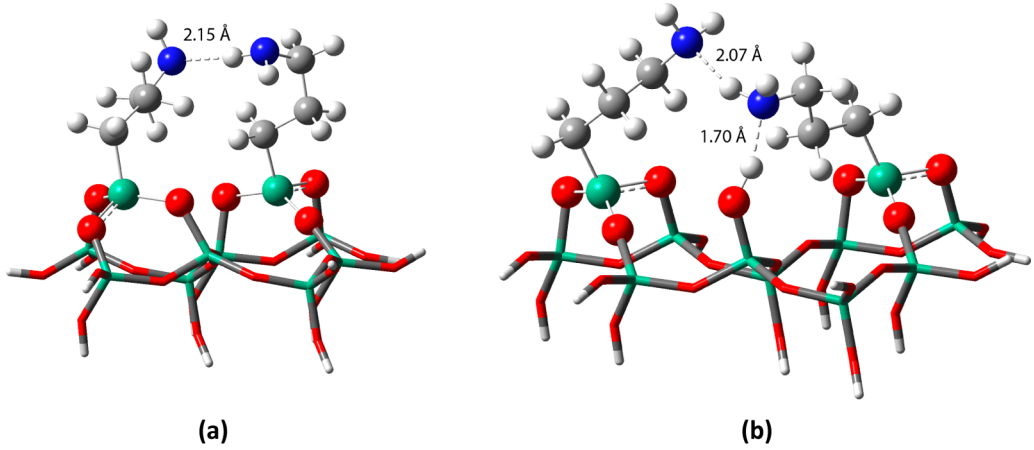

Figure 1. Views of the AFMS@8-T (a) and AFMS@9-T (b) cluster models with APTES functionalization. Spheres and tubes represent fully optimized and fixed atomic positions, respectively.

were determined in a laboratory-made stainless steel volumetric apparatus, with a pressure transducer (Pfeiffer Vacuum, APR 266), equipped with a rotary/diffusion pump system which allowed a vacuum greater than 10^{-2} Pa. The apparatus and adsorption cell temperature was maintained with a water bath (Grant, GD 120) at 25.00 ± 0.05 °C. Before adsorption experiments, the samples were degassed as described above for N_2 adsorption assays. The non-ideality of the gas phase was taken into account using the second and third virial coefficients to calculate the adsorbed amounts. Excess adsorbed amounts determined experimentally were converted to absolute amounts using the gas density and porous volumes of the samples.

2.4. Computational Details. The silica clusters used to model the silica surface are based on the experimental crystallographic structure of alpha-quartz,[39] using the atomic positions of the Si and O, and the bond angles on this accurately known structure. The cluster models are based on eight and nine Si atoms and, following the notation used by López et al.,[40] are from now on named *N*-T models (*N* = 8 or 9, respectively). The 8-T and 9-T models include six and seven surface OH groups, respectively. Dangling bonds at the edges of the cluster models due to elimination of Si atoms were conveniently saturated with H atoms along the O−Si directions of the perfect crystal and imposing an O−H distance equal to 0.96 Å.[41] A pair of the amino-organosilanes considered in this work was then grafted directly on top of the cluster models where OH groups existed, each binding three surface OH groups, to obtain the AFMS@N-T models (Figure 1). Therefore, a surface OH group is left in the case of the AFMS@9-T model (Figure 1b). In both cases, the alkylamines, the SiO_3 moieties binding the alkylamines and, when available, the surface OH group were fully relaxed, while the remaining Si and O atoms were kept frozen at their crystallographic positions. The fixation of some atomic positions provides a simple but effective representation of the mechanical embedding of the solid covalent oxide surface.[40,42] In the case of the calculations involving the interaction of CO_2 with the AFMS@N-T models, the optimization procedure was exactly the same as that described above for the bare cluster models but with the atoms of the chemisorbed CO_2 species also fully optimized. The absence of imaginary values in the frequencies involving the atoms optimized in the different structural models considered in the present work ensured that the structures are true minima on the potential energy surface.

Some comparative calculations without the silica surface were performed by eliminating all the frozen atoms from the AFMS@8-T model shown in Figure 1a. Dangling bonds were saturated as above. In such calculations, all the atoms were fully relaxed with the exception of the terminal OH groups. Also, some comparative calculations were performed for situations were just an amino-organosilane was grafted onto 1-T, 3-T, 8-T, or 9-T models. In the two latter cases, three and four silanol groups are left unreacted on the silica surface.

The M06-2X hybrid functional based on the meta-generalized gradient approximation of Truhlar and Zhao[43,44] and the standard 6-31G(d) basis set,[45,46] with a single polarization function in all the atoms, as included in the Gaussian 09 software,[47] were used in all the calculations. The combination of the M06 family of functionals and Gaussian-type orbitals basis sets with cluster models was found to provide geometries, energies, and frequencies in very good agreement with available experimental data for several systems[48−51] that are challenging for DFT approaches from the lower rungs of the Jacob's ladder of density functional approximations.[52] The M06-2X functional has been suggested for geometry optimization in a guide to small-molecule structure assignment through computation of ^{1}H and ^{13}C NMR CSs.[53] In all calculations, the default integration grids and convergence thresholds in the Gaussian 09 software were employed.[47]

CO_2 can interact with the AFMS surfaces either physically, i.e., physisorption state without establishment of chemical bond(s), or chemically, i.e., chemisorption state with the formation of carbon−nitrogen bonds with the nitrogen atoms of the alkylamines. So, for each cluster model, we have calculated the difference between the M06-2X electronic energies of these two states, i.e., $\Delta E = E_{\text{chemisorbed-state}} - E_{\text{physisorbed-state}}$. From this point onward, ΔE will be named as the stabilization energy.

Nuclear magnetic resonance shielding tensors of the optimized geometries have been computed with the gauge-independent atomic orbital (GIAO) method,[54] also using the M06-2X functional because of the small root-mean-square deviations of the calculated to the experimental ^{1}H (cf. 0.2 ppm) and ^{13}C (cf. 3.2 ppm) CSs found for a large set of organic molecules.[55] The ^{13}C isotropic magnetic shielding tensors calculated for the clusters were subtracted from those calculated for tetramethylsilane (TMS) to obtain the CSs relative to this reference. The calculated CS for CO_2 was 125.2 ppm, comparing with the 124.9 ppm for the experimental value. This small difference between the experimental and calculated values for CO_2 was used to correct the calculated ^{13}C CSs and suggests that the uncertainties associated with the calculated ^{13}C shifts are very probably smaller than the RMSD value above. Encouragingly, the M06-2X/6-31G(d) ^{13}C shift for the carbonyl group of acetic acid with HBs to water (cf. δ_C = 179.5 ppm) was also found to compare very well with the experimental result[56,57] (cf. δ_C = 178.1 ppm also in water). The ^{1}H isotropic magnetic shielding tensors calculated for the clusters were converted to CS relative to TMS by using a linear correlation, to achieve more accurate CS, with a slope of −1.1082 and an intercept of 32.6273.[55] Infrared vibrational spectra of the optimized models were also calculated in this work at the M06-2X/6-31G(d) level of theory, and the obtained wavenumbers were corrected by a scale factor of 0.947.[58]

2.5. Solid-State NMR Measurements. ^{1}H, ^{29}Si, and ^{13}C NMR spectra were acquired on Bruker Avance III 400 and 700 spectrometers operating at B_0 fields of 9.4 and 16.4 T, respectively, with ^{1}H/^{29}Si/^{13}C Larmor frequencies of 400.1/79.5/100.6 MHz and 700.1/139.1/176.1 MHz, respectively. All experiments were performed on double-resonance 4 mm and 2.5 mm Bruker MAS probes, except

DOI: 10.1021/jacs.6b11081
J. Am. Chem. Soc. 2017, 139, 389−408

for the $^{13}C-\{^{14}N\}$ saturation-pulse induced dipolar exchange with recoupling (SPIDER) experiment where a triple-resonance 4 mm Bruker MAS probe was used. Samples were packed into ZrO_2 rotors with Kel-F (4 mm) or Vespel (2.5 mm) caps. Spinning rates between 12 and 35 kHz were employed to record all the spectra (see figure captions for details). ^1H and ^{13}C CSs are quoted in ppm from TMS (0 ppm) and α-glycine (secondary reference, C=O at 176.03 ppm), respectively. ^{29}Si CSs were referenced with respect to the external secondary reference Q8M8 (octa(dimethylsiloxy)silsesquioxane) setting the high frequency signal (left side resonance) to 11.5 ppm.

^1H single-pulse excitation magic angle spinning (MAS) NMR spectra were recorded at a spinning rate of 30 kHz using a pulse width of 2.66 μs (90° flip angle) corresponding to a radio frequency (rf) field strength of ca. 94 kHz. A recycle delay (RD) of 20 s was found to be sufficient and used for all samples.

The ^{13}C CPMAS spectra were acquired under the following experimental conditions: ^1H 90° pulse set to 3.0 μs corresponding to a rf of ~83 kHz; the CP step was performed with a contact time (CT) of 400−2000 μs using a 50−100% RAMP shape at the ^1H channel and using a 50 kHz square shape pulse on the ^{13}C channel; RD was 5 s. During the acquisition, a SPINAL-64 decoupling scheme was employed using a pulse length for the basic decoupling units of 5.6 μs at rf field strength of 83 kHz.

The $^1H-^{13}C$ CP/LG-CP HETCOR spectra were acquired using frequency-switched Lee−Goldburg (FSLG) ^1H homonuclear decoupling during the indirect dimension (t_1). Either CP or LG-CP was employed to achieve ^1H to ^{13}C magnetization transfer. The CP conditions were the same as indicated above. For LG-CP the conditions used were CT of 300 and 2000 μs; ^{13}C rf amplitude ramped at 50−100%, and a rf amplitude for ^1H spin-lock of 50 kHz at a LG offset irradiation of $-50000/\sqrt{2} = -35354$ Hz. 50 t_1 points with 1−2k scans each were recorded along the indirect dimension. A ^1H rf field strength of 83 kHz and asymmetric LG offsets of 54 925 Hz and −62 925 Hz were used for FSLG decoupling employing a LG pulse of 9.8 μs. The indirect dimension dwell time was set equal to four FSLG blocks (78.4 μs). Quadrature detection in t_1 was achieved by the States-TPPI method. The ^1H CSs were corrected assuming a scaling factor of $1/\sqrt{3}$ for FSLG decoupling.

The $^1H-^{29}Si$ CP HETCOR spectra were also acquired using FSLG decoupling during the indirect dimension (t_1) employing the same experimental conditions as described above. The CP conditions were: CT of 2500 μs; ^{29}Si rf power amplitude ramped at 50−100% and a ^1H spin-lock rf amplitude of 50 kHz. 32 t_1 points with 7800 scans each were recorded along the indirect dimension.

$^{13}C\{^{14}N\}$ SPIDER NMR experiments were performed at 9.4 T using a spinning rate of 5 kHz. During the $^{13}C-^{14}N$ heteronuclear recoupling evolution, eight rotor periods were employed (1.6 ms), while during the central ^{14}N irradiation time (SPIDER dephasing), a train of ^{14}N saturation pulses of 4 μs using an rf field strength of 30 kHz alternated with windows of 2.5 μs were applied during four rotor periods (0.8 ms). The 180° pulse length on ^{13}C was set to 6 μs, and 70 kHz of ^1H decoupling power was used during the recoupling, ^{14}N saturation, and acquisition periods. Additional details about the SPIDER pulse sequence may be found elsewhere.[59]

Variable contact-time measurements were recorded using a ^1H CP power level (square shape) of 35.7 kHz and ^{13}C CP power level of 42 kHz. Spectra were recorded using 17 distinct contact times: 50 μs, 100 μs, 200 μs, 300 μs, 500 μs, 700 μs, 1 ms, 2 ms, 4 ms, 6 ms, 8 ms, 10 ms, 13 ms, 16 ms, 20 ms, 25 ms, and 30 ms. A total of 2000 scans were accumulated for each measurement.

All reported ^1H NMR CSs extracted from the HETCOR spectra have an average estimated error of ±0.5 ppm due to the scaling factors used for FSLG decoupling to calibrate the ^1H CSs at the indirect dimension. Further relevant experimental details can be found in the corresponding figure captions.

The preparation of the sample was performed in a laboratory-made high-vacuum line, connected to a turbomolecular pumping station (HiCube 80, Pfeiffer Vacuum), capable of vacuum greater than 10^{-2} Pa. After packing samples in zirconia rotors, they were put in a laboratory made borosilicate glass cell adapted from the description in the literature[60] and capable of heating the rotor to 150 °C under vacuum. The heating was performed with a laboratory made oven connected to a power controller (Eurotherm 3116), and the temperature was measured with a thermocouple. The samples were first degassed and then heated; usual heating program was a ramp of 5 °C/min followed by 2 h at 150 °C under vacuum, except where noted differently in the text. After cooling down under vacuum, $^{13}CO_2$ (Cortecnet, 99 atom % ^{13}C; <3 atom% ^{18}O) was introduced from the canister connected to the vacuum line and the cell up to the desired pressure, measured with a capacitance transducer (MKS instruments, Baratron 722B). The equilibration of the $^{13}CO_2$ pressure was allowed for at least 30 min. After, the cell was filled with helium (Air Liquide, 99.999%) up to the atmospheric pressure, if needed. The rotor was closed inside the cell, which is similar to that developed for studying zeolites as described elsewhere,[61] and only then the cell was open to remove the prepared rotor for NMR measurements. For experiments with controlled partial pressure of water; water vapor was introduced into the cell after the thermal treatment of the samples from a glass container with liquid water connected to the vacuum line by opening a valve on the glass container. Prior to use, deionized water (Millipore Milli-Q) was further purified by freeze−vacuum−thaw cycles. After introduction of water, CO_2 and helium were introduced in the cell as described above, and the preparation proceeded accordingly.

3. RESULTS AND DISCUSSION

3.1. Porosity and Thermal Properties of the Materials.

The porosity of SBA-15 before and after functionalization with amines was assessed by low-temperature nitrogen adsorption (Figure S1 and Table S1). The parent SBA-15 sample presented an adsorption isotherm of type IV according to IUPAC classification,[62] typical of an ordered mesoporous material. The presence of micropores was investigated by a detailed analysis of the nitrogen adsorption isotherm with the α_s-plot method,[36,63] using nonporous hydroxylated silica as reference material,[63] giving a small micropore volume of 0.011 cm^3g^{-1} (about 1% of the total pore volume). This is in agreement with previous detailed analysis of the SBA-15 porosity and adsorption properties made by Pires et al.[64] The AFMS materials exhibit the same type of isotherm, but with lower amounts of N_2 adsorbed. This is to be expected, since amine functional groups occupy the pore volume, implying lower available adsorption space that is quantified by the total pore volume of the samples (V_{tot}, Table S1). Samples with TMMAP and N-3 functional groups presented the highest decrease (53%) and the sample with ATPES the lowest (36%). This correlates with the fact that the latter molecule is smaller than the former two. The case with 3-DEAPTES presented an intermediate decrease in V_{tot} (46%), although this is the bulkiest functional group among those tested (see Scheme 1). This result is most likely a consequence of the lowest degree of grafting achieved with this sample compared to the other cases (Table S1). The similar shape of all the isotherms confirms that the main characteristics of the SBA-15 porosity were preserved upon functionalization. A small displacement in the position of the hysteresis loop is observed for the amine-functionalized SBA-15 samples, which corresponds to a slight narrowing of the mesopores (Figure S1 inset). In fact, it can be observed that the maxima of the pore size distributions decrease upon functionalization and are more pronounced for samples with bulkier groups, except for the 3-DEAPTES case. The decrease in pore size indicates that a significant part of the functionalization process has occurred inside the mesopores of the SBA-15 material. The C factor from the BET equation is also given in Table S1, although this parameter is only relevant

DOI: 10.1021/jacs.6b11081
J. Am. Chem. Soc. 2017, 139, 389−408

to correlate the N_2 and CO_2 physisorption, when no chemisorption is occurring.[65]

The thermal stability of the materials in air was characterized by TG-DSC (Figure S2), and data were used to determine the organic content of the samples. A first endothermic peak up to about 100 °C, associated with significant mass loss, followed by a small plateau centered at about 150 °C is always observed in all functionalized samples. This is also observed on the nonfunctionalized SBA-15 (Figure S2) and is attributed to desorption of water and gases from the pores. Thus, the mass at this temperature was considered as the reference for the clean solids. Above 150 °C, the parent SBA-15 does not display a significant mass loss, and no heat flow peak is observed (endo or exothermic), indicating that the material is stable up to 500 °C. For the amine-functionalized materials, the observed mass loss and heat flow curves evidencing an exothermic peak indicate the decomposition of the organic fraction of the materials in air, which starts above 200 °C (Figure S2), since SBA-15 is stable at this temperature range. The shape of the curves is slightly different for each functionalized material, but they all seem to indicate that most of the decomposition of the organic part occurs up to about 500 °C. For one of the functionalized materials (TMMAP@SBA-15), a second thermal analysis was made in the sample obtained at the end of the first analysis. The obtained mass loss and heat flow curves are similar to those of the bare SBA-15 material, which confirms that after the first thermal cycle the organic fraction is removed from the samples and the obtained solid is essentially a porous silica substrate. Considering that the mass loss between 150 and 500 °C arises effectively from the removal of the organic part, the samples can be compared regarding the amount of organic fraction that was introduced by the functionalization procedure. Other authors have also used this procedure to quantify the amine functionalization of silicas.[22,66,67] The values presented in Table 1 indicate that upon increasing the functional group from APTES to larger organic groups, an increase in the organic fraction of the materials is obtained, which corresponds to higher mass losses. The molar ratio of the organic amino-organosilane precursors was maintained constant during the synthesis of the materials. Thus, assuming a similar accessibility to the pores of SBA-15, it can be expected that amino-organosilanes with larger organic parts would give materials with higher organic fraction. However, results in Table 1 show that this is not the case. For instance, TMMAP@SBA-15 and N-3@SBA-15 present similar mass losses, i.e. similar organic fractions, but the N-3 organic group is bigger than TMMAP. Moreover, 3-DEAPTES@SBA-15 contains a lower organic fraction than TMMAP@SBA-15 and N-3@SBA-15, although 3-DEAPTES is the biggest of the organic groups tested. This suggests that during the functionalization process, the bulky 3-DEAPTES struggles to diffuse inside the pores and/or has more difficulty to achieve efficient packing inside the pores, compared to the other amino-organosilanes. Nevertheless, other effects, as for instance the basicities of the amines in the grafting reactions, may also play an important role in the observed loading difference. It is important to note that the decrease in surface area (A_{BET}) shown in Table S1 is related with the increase in organic faction depicted in Table 1. This is expected because the organic groups are occupying adsorption space inside the SBA-15 pores. Considering the initial surface area of the parent SBA-15 and the amine content on the materials, an estimation of the average amine density on the surface can be obtained, see Table 1. These values will be discussed in the context of the computer simulations presented below. The density of amines in the case of the APTES@SBA-15 sample (2.37 molecules/nm^2) is close to the density of 2.4 molecules/nm^2 obtained by other authors using similar synthesis conditions, i.e., similar amount of APTES per gram of SBA-15.[10,67,68] Note that the latter densities are larger than those found in mesoporous silicas with narrower pores, like MCM-41 and FSM-16, where the amount of APTES that can be loaded under similar synthesis conditions is below 1 molec./nm^2.[69]

Table 1. Mass Loss, Nitrogen Content, and Grafting Density on the Samples Obtained from TG-DSC Data

sample	$\Delta m/m_i$[a] %	N content mmol/g	grafting density molec./nm^2
SBA-15	−1.3		
APTES@SBA-15	−11.6	2.82	2.37
3-DEAPTES@SBA-15	−15.5	1.59	1.34
TMMAP@SBA-15	−17.0	3.09	2.60
N-3@SBA-15	−16.5	3.93	1.65

[a]Difference between mass at 150 °C (clean solid) and mass at 500 °C (Δm) divided by the mass at 150 °C (m_i).

3.2. Carbon Dioxide Adsorption. Samples were also characterized for their CO_2 adsorption capacity. CH_4 was also measured to better illustrate the affinity of the material for CO_2, since this gas does not interact chemically with amines. Adsorption isotherms of CO_2 and CH_4 up to 1000 kPa are shown in Figure S3. The observed changes in pore size and volume, discussed above, can induce by themselves changes in the adsorption properties of the samples. However, contrary to what is observed for methane, the functionalization of the SBA-15 increases significantly the adsorbed amounts of CO_2 at low pressures, except as expected for the 3-DEAPTES@SBA-15 (tertiary amine), which demonstrates the high affinity of these materials for CO_2. Adsorption isotherms become steeper in the low-pressure regime upon functionalization with primary and secondary amine groups (APTES@SBA-15, TMMAP@SBA-15, and N-3@SBA-15). As will be apparent from the discussion of the NMR results at variable CO_2 pressure (section 3.3.3), some physisorbed CO_2 is in equilibrium with chemisorbed CO_2 even at low pressures. Thus, the relation between the amount of amines in the materials and the amount of chemisorbed CO_2 cannot be calculated from the isotherms because, even at low pressures, there is a fraction of CO_2 species that is not interacting chemically with the substrate (i.e., physisorbed species). The detailed discussion of the adsorption results and their implications in methane upgrading is outside the scope of the present work and will be presented elsewhere. The important finding in the present context is to demonstrate that the functionalization of the SBA-15 was effective to produce materials with high affinity and adsorption capacity for CO_2. The differences observed in the APTES@SBA-15 and TMMAP@SBA-15 isotherms at low pressures will be rationalized in the discussion of the ^{13}C SSNMR spectra recorded at variable $^{13}CO_2$ pressures.

3.3. SSNMR Characterization of Chemi- and Physisorbed CO_2 Species. *3.3.1. General Consideration.* Several studies of AFMS exist in the literature, with only a few of them employing NMR to identify chemisorbed CO_2 species resulting from chemical reactions between amines and CO_2. Some authors identified the typical amide functional groups produced

DOI: 10.1021/jacs.6b11081
J. Am. Chem. Soc. 2017, 139, 389−408

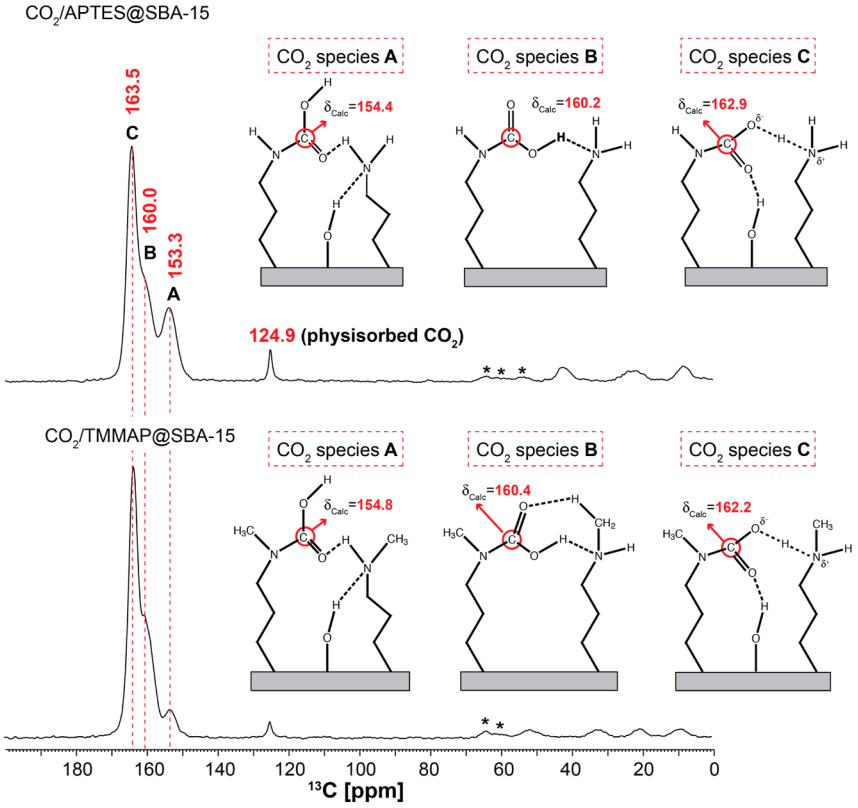

Figure 2. ^{13}C CPMAS NMR spectra of APTES@SBA-15 and TMMAP@SBA-15 materials, recorded at 9.4 T, after exposure to $^{13}CO_2$ (100 kPa). **A**, **B**, and **C** denote the three resonances attributed to the chemisorbed CO_2 species. Asterisks denote spinning sidebands. Sketches of optimized configurations (see below) incorporating the computed CSs are also provided.

upon CO_2 adsorption, and it is generally accepted that the formation of ammonium carbamate ion pair occurs primarily based on solution-state chemical reactions of amines with CO_2.[14] In the solid state, the assignment of the chemisorbed CO_2 species and of the HB interactions formed is, however, very difficult to prove experimentally. In addition, it is hard to detect ^{13}C resonances, associated with dilute chemisorbed CO_2 species if ^{13}C-enriched CO_2 gas is not used, as previously shown by our group.[27]

To perform this NMR characterization study, all the samples were packed into the NMR sample holder in a controlled atmosphere (see experimental section for further details). It was found that such rigorous sample handling was of the upmost importance as it enabled the observation of certain ^{13}C resonances that otherwise would not be detected. Perhaps this is the reason why the herein newly identified chemisorbed CO_2 species, associated with the resonance at δ_C = 153.3 ppm, found in this work, was not reported before (see text below).

NMR experiments were conducted on the four amine-grafted SBA-15 materials (Scheme 1) loaded with ^{13}C-enriched CO_2 and labeled as CO_2/**X**@SBA-15 (with **X** being APTES, TMMAP, N-3, and 3-DEAPTES). However, we focus a detailed study in two of them, i.e., CO_2/APTES@SBA-15 and CO_2/TMMAP@SBA-15, as these two materials are representative of the two types of amines (primary and secondary) that can actively bind CO_2 in the absence of moisture, and present similar amine contents (difference is ~7%, cf. Table 1), compared to the other bulkier amines tested. The N-3 and 3DEATPES AMFS will be mentioned when absolutely necessary to compare the presence of certain resonances that showed in the spectra of APTES/TMMAP@SBA-15 materials. Note that we have intentionally tried to load SBA-15 with as much amines as possible for NMR sensitivity enhancement purposes and to increase the probability of HB formation to enable their detection by NMR. The amines were grafted into SBA-15 synthesized from the same batch, to minimize differences in the final materials due to the silica substrate. Although, a comprehensive study of how the different intermolecular interactions change with different amine loadings is out of the scope of this work, we compare the amine loading effect in NMR spectra for only a few special cases.

3.3.2. Identification of Chemisorbed CO_2 Species by 1D ^{13}C (CP)MAS NMR. Figure 2 shows the ^{13}C CPMAS spectra of CO_2/APTES@SBA-15 and CO_2/TMMAP@SBA-15 with the resonances corresponding to the grafted alkyl chains appearing below 60 ppm. The peak at $\delta_C \approx 125$ ppm corresponds to *physisorbed* CO_2, while the three ^{13}C resonances appearing in the region between 150 and 170 ppm are typically associated with amide carbons formed upon CO_2 chemisorption with the amines, the latter henceforth labeled as **A**, **B**, and **C**. ^{13}C CPMAS spectra of SBA-15 samples grafted with other bulkier amines, at lower loadings, were also recorded but will not be discussed here (Figure S4). The assignment of physisorbed CO_2 was confirmed by comparing a ^{13}C CPMAS NMR and a ^{13}C single-pulse NMR spectrum of $^{13}CO_2$ adsorbed in pure SBA-15 (Figure S5). A single ^{13}C resonance only appears in the latter spectrum as the mobile nature of $^{13}CO_2$ gas prevents the signal to appear in the CPMAS spectrum. We have previously identified carbamic acid species appearing at $\delta_C \approx 160$ ppm (resonance **B**, Figure 2) and studied its pressure and thermal stability.[27] However, herein we report on newly detected

DOI: 10.1021/jacs.6b11081
J. Am. Chem. Soc. 2017, 139, 389−408

chemisorbed CO_2 species, observed in the studied materials. This new species exhibits a ^{13}C resonance of $\delta_C \approx 153$ ppm (resonance **A**, Figure 2), which was observed *only* under extremely dry conditions. In fact, we recorded a ^{13}C CPMAS spectrum of CO_2/APTES@SBA-15 after adsorbing merely 133 Pa partial pressure of water vapor. Subsequently, we waited for the CO_2 equilibrium pressure to be reached. In such conditions, resonance **A** ($\delta_C \approx 153$ ppm) vanished completely (Figure 3).

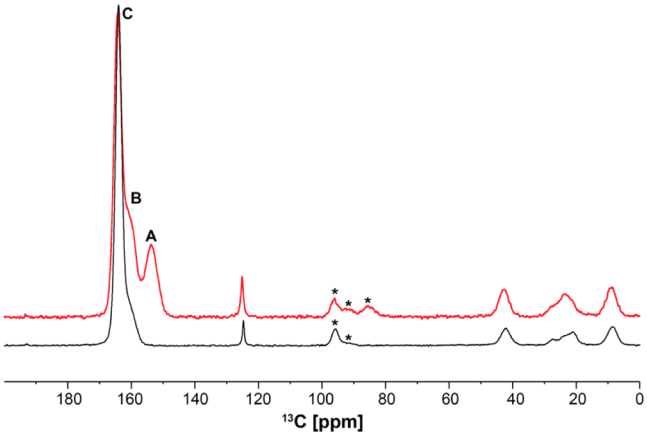

Figure 3. ^{13}C CPMAS NMR spectra of CO_2/APTES@SBA-15 recorded at 16.4 T, under dry (top) and humid (133 Pa partial pressure of water vapor) conditions (bottom), in the presence of 100 kPa of CO_2. **A**, **B**, and **C** denote the three resonances attributed to the chemisorbed CO_2 species. Asterisks denote spinning sidebands.

The same phenomenon was observed in all AFMS materials even when they were exposed to extremely low amounts of water vapor. The extreme sensitivity of species **A** to water is thus in sharp contrast to the stability of species **C** (resonance at $\delta_C \approx 164$ ppm) and species **B** (resonance at $\delta_C \approx 160$ ppm), whose ^{13}C signals remain unchanged under moist conditions. An obvious question arises: Why is species **A** vanishing from the ^{13}C CPMAS spectra of amine-grafted SBA-15 samples when water is present even in extremely low amounts?

Recently, a new chemisorbed CO_2 species, named silylpropylcarbamate, was identified based on *in situ* FTIR studies and was assigned to surface-bonded carbamate moieties formed only at relatively low amine density conditions.[11,18,20] These studies suggest that this particular species is only formed under dry conditions, and, coincidently, we also detected a new species (species **A**, Figure 3) in such conditions. However, the materials used in our study exhibit amine loadings in the range from 1.59 to 3.93 mmol N/g, which is higher than amine densities mentioned in previous studies.[11,18,20] CO_2 and isotopically labeled $^{13}CO_2$ were employed to facilitate the assignment of FTIR bands attributed to specific chemisorbed CO_2 species such as silylpropylcarbamate.[20] However, unambiguous FTIR assignment of several possible formed species proved to be difficult mainly due to significant overlapping of the vibrational bands associated with distinct species.

Although clear experimental evidence about the nature of CO_2–amine interactions is still not straightforward to obtain, an optimized model of silylpropylcarbamate (Figure S6 right) yielded a computed ^{13}C CS of $\delta_C \approx 151.4$ ppm. This value is close to the experimental resonance observed at $\delta_C \approx 154$ ppm, which could thus provide the first experimental NMR evidence of the existence of such species. Nevertheless, according to literature, this species is supposed to be very stable under dry conditions and should not disappear with vacuum or temperature treatment.[20] To test the stability of the newly detected species, we exposed CO_2/APTES@SBA-15 to vacuum conditions and monitored the intensity of the ^{13}C resonance **A**. After 5 min of high vacuum, resonance **A** reduced to the intensity of the diluted methylene carbons from the alkyl chain (Figure 4). This result suggests that species **A** may be another

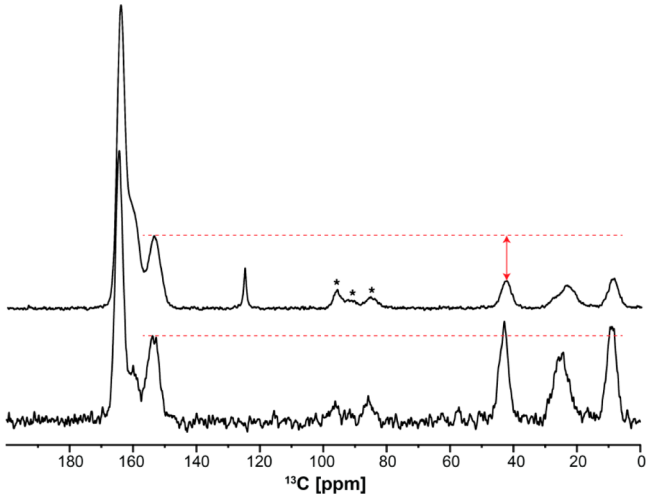

Figure 4. ^{13}C CPMAS NMR spectra of CO_2/APTES@SBA-15 recorded at 16.4 T: (top) immediately after exposure to 100 kPa $^{13}CO_2$ and (bottom) immediately after exposure to 100 kPa $^{13}CO_2$ for 1 h followed by 5 min vacuum. Dashed lines illustrate the difference in intensities between resonance **A** and the alkyl region. Asterisks denote spinning sidebands.

"less stable" chemisorbed CO_2 species since its signal decreases significantly under vacuum, similar to species **B** and **C**. In fact, this experiment demonstrates that all chemisorbed CO_2 species formed (**A**, **B**, and **C**) are very unstable regarding the partial pressure of CO_2 (Figure 4), suggesting that their chemical nature is very labile. Although the calculated ^{13}C CS value of the silylpropylcarbamate is close to the experimental one, we herein propose another structure which may explain the ^{13}C resonance shift to lower frequencies (**A**) compared to the most abundant species (**B** and **C**). Our results point toward the presence of isolated carbamic acid species, i.e., species with its N-COOH group *not* engaged in hydrogen bonding via the OH. According to theoretical models presented in section 3.4, the carbonyl group (N-COOH) of such species is estimated to resonate at $\delta_{calc}(^{13}C) \approx 154.0$ ppm (for CO_2/APTES@SBA-15) and $\delta_{calc}(^{13}C) \approx 154.8$ ppm (for CO_2/TMMAP@SBA-15). To support the assignment of the **A** species, we have also carried out a ^{13}C CPMAS NMR experiment of CO_2/APTES@SBA-15 (Figure S7) in a sample with low amine content (1.1 mmol/g). The spectrum reveals that resonance **A** is now dominant at low amine coverage. The other two resonances have their intensities drastically reduced. This supports the idea that the CS at about 153 ppm can be attributed to a species where the OH of the carbamic acid is not engaged in HB, in accordance with DFT calculations in section 3.4.

3.3.3. ^{13}C CPMAS NMR Spectra Recorded at Variable Partial CO_2 Pressures. In order to understand which chemisorbed species are forming in the first place, we have carried out ^{13}C CPMAS experiments at variable $^{13}CO_2$ partial pressures from 0.13 to 101 kPa on CO_2/APTES@SBA-15 and CO_2/TMMAP@SBA-15. The ^{13}C CPMAS spectra shown in

DOI: 10.1021/jacs.6b11081
J. Am. Chem. Soc. 2017, 139, 389–408

Figure 5 were normalized with respect to the intensity of the propylamine carbons to obtain a fair comparison between

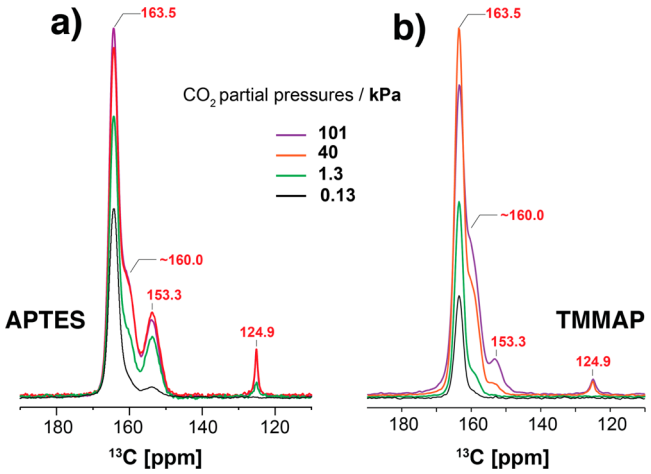

Figure 5. ^{13}C CPMAS NMR spectra of (a) CO_2/APTES@SBA-15 and (b) CO_2/TMMAP@SBA-15 recorded at 9.4 T and variable $^{13}CO_2$ partial pressures under dry conditions. Peak intensities were normalized with respect to the alkyl carbon signals for a fair comparison. Asterisks denote spinning sidebands.

NMR spectra at all CO_2 partial pressures. At the lowest pressure of 0.13 kPa, species **C** appearing at $\delta_C \approx 164$ ppm is the most abundant in all materials. The NMR spectrum of TMMAP@SBA-15 clearly shows that at the lowest pressure of CO_2 almost all of the population of chemisorbed CO_2 species are of type **C** (Figure 5). Increasing the CO_2 pressure up to 1.3 kPa enhances the intensity of species **B**. The peak corresponding to species **A** is only noticeable at the two highest CO_2 pressures (40 and 101 kPa). In the case of CO_2/APTES@SBA-15, all species seem to be simultaneously populated even at CO_2 partial pressure as low as 1.3 kPa (Figure 5). It is worth mentioning that at 1.3 kPa, the resonance assigned to physisorbed CO_2 ($\delta_C \approx 125$ ppm) is not yet visible in the case of CO_2/TMMAP@SBA-15, while it already appears in the spectrum of CO_2/APTES@SBA-15. As the quantity of grafted amines is similar in both cases (Table 1), it appears that at 1.3 kPa there is less physisorbed CO_2 in CO_2/TMMAP@SBA-15 than in CO_2/APTES@SBA-15. This is in agreement with the fact the former shows higher CO_2 affinity than the latter since it shows a steeper adsorption isotherm (Figure S3). In fact, at 1.3 kPa the estimated adsorbed amounts from the isotherms are 0.33 and 0.05 mmol g^{-1}, for CO_2/TMMAP@SBA-15 and CO_2/APTES@SBA-15, respectively. Thus, considering that these materials have similar amine loadings (Table 1), the combined NMR and adsorption data indicate that TMMAP@SBA-15 is much more effective at binding CO_2 than APTES@SBA-15. There is one detail that stands out from the analysis of Figure 5; peak **C** decreases noticeably from 40 to 100 kPa in CO_2/TMMAP@SBA-15, while the intensities of peaks **A** and **B** shows the opposite trend, whereas the peak intensities of all the species (**A**, **B**, and **C**) in CO_2/APTES@SBA-15 show the same trend and are essentially maintained. This could indicate that at even higher CO_2 pressures (not attainable in this work) the population distribution among the distinct chemisorbed sites may still considerably change.

To check for differences in the H···C dipolar interactions among the three distinct chemisorbed CO_2 species from CO_2/APTES@SBA-15, variable contact-time CP experiments were performed. Figure S8 depicts the resulting experimental CP kinetic curves along with the fitted curves (solid lines) of four carbon species, i.e., the three CO_2 chemisorbed species and physisorbed CO_2 (ca. 125 ppm). It can be seen that all species give rise to distinct CP build-up rates (initial part of the CP profile), which are to a first approximation, independent of any $T_{1\rho}$ effects and may be used to estimate the polarization transfer time, T_{HC}. The fit of the CP profiles yielded T_{HC} values of ca. 1.46, 0.86, 1.09, and 4.06 ms for species **A**, **B**, **C** and physisorbed CO_2, respectively (Table S2). In general T_{HC} depends on the number of protons in the functional group involved in the polarization process, their disposition, and on the mobility of the group. However, assuming similar proton distribution among the three chemisorbed CO_2 species (this assumption holds if an approximately homogeneous grafting is also presumed), differences in T_{HC} values may be tentatively attributed to differences in molecular rigidity, which thus lead to divergent H···C dipolar couplings. Following this argument, **B** species possess the strongest H···C dipolar interaction (i.e., shortest T_{HC} values), while species **A** shows the inverse behavior. Comparing the T_{HC} values (Table S2), the HB strengths involved in the three chemisorbed CO_2 species, in order of increasing strengths, correspond to **A**, **C**, and **B**. This is in remarkable agreement with the corresponding HB lengths obtained from the DFT optimized molecular models of these three species (see Figure 12), which depict species **B** having the shortest HB length [compare $d_{C=O\cdots HN}$ = 1.65 Å (Figure 12b) with $d_{C=O\cdots HN}$ = 2.58 Å (Figure 12a) and $d_{OH\cdots N}$ = 1.71 Å in Figure 12c] and with the results from the topological analysis reported in Table S3.

The T_{HC} value of physisorbed CO_2 is obviously expected to be the longest ($T_{HC} \approx 4.06$ ms) as this species is far less rigid than chemisorbed CO_2 species. In contrast, short T_{HC} values between 40 and 130 μs (Table S2) were obtained for the protons from the three alkyl CH_2 groups, which is to be expected for carbons with directly attached protons.

3.3.4. Identifying Amine···Chemisorbed CO_2 Species through N···C Dipolar Interactions. The chemisorbed CO_2 species observed in the ^{13}C CPMAS NMR spectra are the result of amines acting as nucleophilic agents that readily attack the CO_2 carbonyl and form a new N−C covalent bond. However, correlation between species **A** and the formation of such a bond is not self-evident. Namely, there are several studies referring to various $-CO_x$ species (e.g., carbonates, bicarbonates, etc.) that do not involve a N−C bond.[2,23,70,71] To address this issue, we have performed a ^{13}C-{^{14}N} SPIDER[59] experiment, which probes C···N dipolar couplings and allows us to identify carbons bonded to nitrogen. This $^{13}C\{^{14}N\}$ dipolar dephasing technique has been very successful in characterizing humic substances.[72] In practice, only the ^{13}C resonances corresponding to carbons engaged in C−N bonds are retained in this type of experiment. Figure 6 shows the $^{13}C\{^{14}N\}$ SPIDER difference ($\Delta S = S_0 - S$) spectrum of APTES@SBA-15 proving that all three ^{13}C resonances appearing in the 150−170 ppm region correspond to N−C linkages involving CO_2. The reference spectrum S_0 (without ^{14}N irradiation pulses) and the spectrum S (with ^{14}N irradiation) are also shown in Figure 6. In this experiment, the partially dephased carbon signals in S are compared with the carbon signals in the S_0 spectrum which is obtained without ^{14}N irradiation. The resulting difference spectrum ΔS thus shows ^{13}C resonances exclusively from carbons bonded to nitrogens. ^{13}C spins that are not in close

DOI: 10.1021/jacs.6b11081
J. Am. Chem. Soc. 2017, 139, 389−408

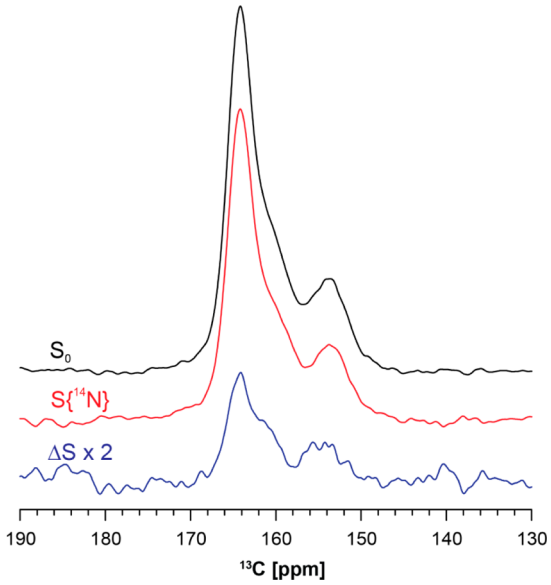

Figure 6. $^{13}C\{^{14}N\}$ SPIDER NMR of CO_2/APTES@SBA-15 recorded at 9.4 T: (top) reference spectrum S_0, (middle) dephased spectrum S, and (bottom) difference spectrum ΔS.

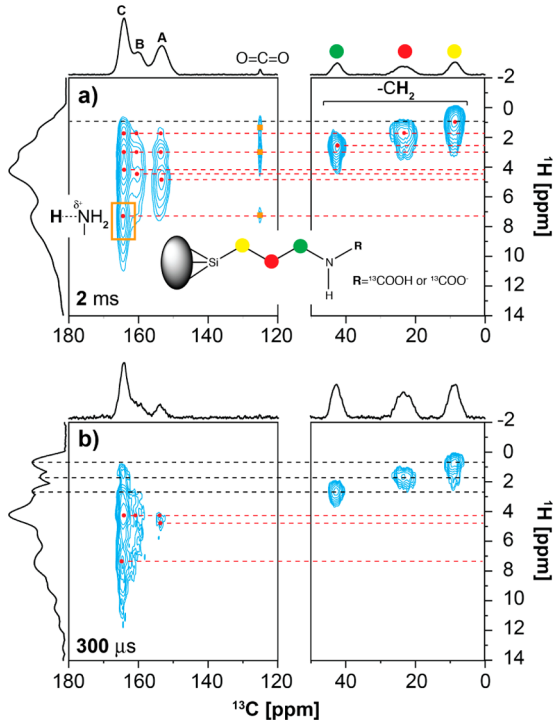

Figure 7. $^{1}H-^{13}C$ HETCOR NMR spectra of CO_2/APTES@SBA-15 recorded at 16.4 T using (a) a CT(LG-CP) = 2 ms and (b) a CT(CP) = 0.3 ms. Additional parameters provided in experimental section.

proximity to ^{14}N spins will not be influenced by ^{14}N irradiation and will be differenced out in the spectrum Δ*S*. The SPIDER experiment thus confirms that the species **A** at ca. 153 ppm is also an adduct of amine and $^{13}CO_2$, which produces a new N–C bond. Besides, we can refute the possibility that ^{13}C resonances **A**, **B**, and **C** originate from carbonate or bicarbonate species as such species do not contain nitrogen atoms. Therefore, it is safe to assume that carbonate or bicarbonate species were not formed under the conditions used.

3.3.5. Probing Intermolecular Interactions Using 1D ^{1}H NMR and 2D $^{1}H-X$ (X = ^{13}C, ^{29}Si) HETCOR Experiments. It has been reported that ammonium carbamate ion pairs can be formed and that cooperative effects involving amine clustering are necessary to produce maximum chemisorption of up to 0.5 CO_2 molecules per amine.[34] IR of cluttered and isolated amines upon CO_2 uptake have been reported.[10,22] Our NMR measurements, presented above, show that several CO_2 adducts are actually formed and the number of possible intermolecular interactions makes their unequivocal assignment extremely complicated. Both, the formed chemisorbed CO_2 species and the silanol groups present at the pore surface contain hydrogens, which can be engaged in HBs with surrounding groups. By using ^{13}C-labeled CO_2 adsorbed in the studied materials at controlled pressure and moisture levels we were able to acquire 2D $^{1}H-^{13}C$ HETCOR spectra from which $^{1}H\cdots^{13}C$ proximities can be estimated. Figure 7 shows the $^{1}H-^{13}C$ HETCOR NMR spectra of CO_2/APTES@SBA-15 recorded at two distinct contact times (CTs). The spectrum shown in Figure 7a was recorded using LG-CP to polarize more distant carbon resonances avoiding the effect of ^{1}H spin diffusion during longer CT. The spectrum shown in Figure 7b was obtained by the same experiment but using a shorter CT to select cross-peaks associated with one-bond C–H, i.e., protons directly attached to carbons. The former spectrum displays a large number of distinct proton environments associated with the three observed amine-CO_2 chemisorbed species **A**, **B**, and **C**. The CH_2 protons associated with the propylamine chain are clearly separated at $\delta_H \approx 0.7$, 1.6, and 2.7 ppm in the indirect dimension of the $^{1}H-^{13}C$ HETCOR spectrum. This is also consistent with the proton resonances in the ^{1}H MAS NMR spectrum recorded at a MAS rate of 35 kHz (Figure S9). The cross-peaks representing C···H connectivities in the 150–170 ppm ^{13}C region are however not so straightforward to analyze. Interestingly, comparing spectra (a) and (b) recorded at different contact times (Figure 7), we can conclude that the high frequency ^{1}H resonance centered at $\delta_H \approx 7.3$ ppm is correlated only with the **C** resonance. ^{1}H CSs, in this region, are usually associated with protonated amines (generated from either alkylammonium carbamate species or zwitterions) or hydrogen-bonded proton species involving amines. Also, such ^{1}H environments do not appear in the $^{1}H-^{13}C$ HETCOR spectrum of APTES@SBA-15 without adsorbed CO_2 (data not shown). This experiment suggests that this dominant cross-peak is likely due to chemisorbed CO_2 species in a region of cluttered amines, i.e., requiring the presence of neighboring amines to allow proton transfer from carbamic acid moieties to amine groups. Other strong cross-peaks, which may be associated with a number of different ^{1}H species are observed at $\delta_H \approx 2.9$, 4.2–4.4, and 4.8 ppm (see horizontal dashed lines in Figure 7).

Moreover, many of the protons (e.g., aliphatic, amide, amine, carboxylic acid protons) associated with the amine/carbamate molecules may overlap the silanol ^{1}H resonances. From the ^{1}H MAS NMR spectrum of as-prepared SBA-15 (parent material) it may be shown that silanol signals resonate at $\delta_H \approx 1.8$ and 2.9 ppm (Figure S10) but, naturally, CSs values will change if they engage in HBs.

Regarding the water-sensitive species **A**, the cross-peak at $\delta_H \approx 4.8$ ppm is the only resonance that persists at very short CT (Figure 7b) and may only be associated with non-hydrogen-bonded NH amide or COOH carboxylic acid protons. These functional groups can easily form HB networks; however, if that

DOI: 10.1021/jacs.6b11081
J. Am. Chem. Soc. 2017, 139, 389–408

was the case, a cross-peak involving this species would have been observed at highly deshielded ^{1}H CSs (i.e., higher CS values). It is well known that such functional groups easily form HBs; for example, amide protons in proteins appear, depending on HB strength, between ∼6 and 10 ppm,[73,74] while −COOH protons typically resonate above 10 ppm and may reach CSs up to 20 ppm in certain molecular systems.[75] Unfortunately, there is little information reported in the literature regarding CS values where such proton donors are not engaged in HBs because in bulk systems these functional groups are usually interacting strongly with neighboring molecules. In our case, the amines may easily interact with each other as the amine loading is dense enough to allow for such interactions, as reported earlier. However, we cannot discard the possibility that certain amine environments, especially chemisorbed CO_2 species associated with resonance **A**, are isolated; the observation of a dominating resonance in dilute APTES-containing SBA-15 (resonance **A**) highly supports this fact (Figure S7). Earlier studies[76] using solution ^{1}H NMR experiments were conducted where different concentrations of a molecule containing an amide group (*N*-methylacetamide) in apolar solvents were used to show that it is possible for the amide proton signal to approach a high-field limiting ^{1}H CS of 4.8 ppm in dilute conditions (i.e., the amide proton is not hydrogen-bonded with a vicinal molecule). On the other hand, a considerable downfield shift occurred at higher solute concentrations, increasing the amide proton resonance to 8.4 ppm.[76] This shows that acidic protons can appear at much lower ^{1}H CS values than what is normally observed upon hydrogen bonding. In section 3.4, we will present quantum mechanical calculations of ^{1}H and ^{13}C CS on different cluster models showing that non-hydrogen-bonded acidic proton can appear at rather low CS values (3.9 and 4.3 ppm in Figure 12a).

3.3.5.1. Experimental Evidence of Strong HB Formation between Carbamic Acid and Amines. The ^{1}H−^{13}C HETCOR spectrum of CO_2/TMMAP@SBA-15 (Figure 8) is very similar to CO_2/APTES@SBA-15 apart from two distinct features. First, the species **B** appearing at $\delta_C \approx 160$ ppm now exhibits a cross-peak at $\delta_H \approx 11.8$ ppm, which was absent in the spectrum of CO_2/APTES@SBA-15 (Figure 7). This indicates that species **B** in sample CO_2/TMMAP@SBA-15 is engaged in the formation of a strong HB, most likely involving the carboxylic proton (N-COOH). Second, the formation of the new carbamic acid N−C bond in a secondary amine (TMMAP) implies that no NH proton is present since this proton is transferred to the newly formed species. In the case of primary amines (APTES), there is still one NH proton remaining upon CO_2 chemisorption. Therefore, comparing the ^{1}H−^{13}C HETCOR spectra of both materials may help us to assign the N−H amide protons as these species are expected to show only in the 2D spectrum of CO_2/APTES@SBA-15. Indeed, in the case of CO_2/TMMAP@SBA-15 there are no detectable ^{1}H resonances approximately between 4 and 6 ppm; strong ^{1}H resonances were however observed in this CS region in the spectrum of CO_2/APTES@SBA-15 (Figure 7), thus indicating that such protons are associated with NH amide groups.

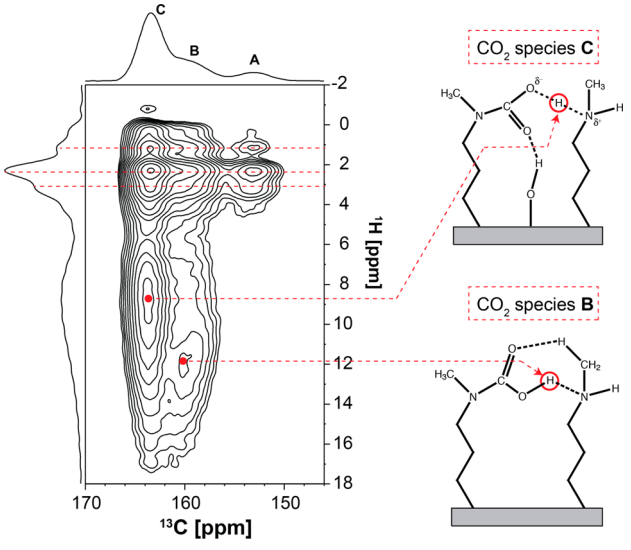

Figure 8. ^{1}H−^{13}C LG-CP HETCOR NMR spectra of CO_2/TMMAP@SBA-15 recorded at 16.4 T using a CT(LG-CT) = 2 ms. Additional parameters provided in experimental section.

In the case of CO_2/TMMAP@SBA-15, species **C** gives a broad cross peak centered at $\delta_H \approx 8.8$ ppm, which we assume is a ^{1}H species analogous to the one appearing at $\delta_H \approx 7.3$ ppm in the spectrum of CO_2/APTES@SBA-15. Nevertheless, we cannot discard the possibility that this broad resonance may also involve protons engaged in various hydrogen-bonding interactions as it will become apparent from the text below.

To help in the assignment task, the ^{1}H−^{13}C HETCOR spectrum of CO_2/N-3@SBA-15, containing a diamine with primary and secondary amine groups was also recorded (Figure S11). It indicates that the presence of both amine groups in the same alkyl chains results in a spectrum which exhibits "an approximate summation" of features observed in the spectra corresponding to the primary (CO_2/APTES@SBA-15) and secondary (CO_2/TMMAP@SBA-15) amines. Figure S11 shows that the ^{1}H resonance at $\delta_H \approx 11.8$ ppm is found again, correlated to **B**, as observed in the case of TMMAP (cf. Figure 8). These findings suggest that alkyl chains containing secondary amines (N-3 and TMMAP) might involve similar interactions upon CO_2 adsorption, regardless of their different amine loading contents (see Table 1).

3.3.5.2. Identification of Proton Species in H/D-Exchanged SBA-15 Grafted with Amines. This cluttered ^{1}H region (between 1 and 5 ppm) in the spectra shown in Figure 7 and Figure 8, is of great importance and its resolution may help to understand the nature of the corresponding C···H interactions. To decipher and assign the protons in this region, we performed a series of NMR experiments on the original and deuterated materials. We have thus exposed the APTES@SBA-15 to D_2O for 24 h to induce H/D exchange and subsequently dried/degassed the materials for 2 h at 150 °C under high vacuum. $^{13}CO_2$ was then adsorbed on the deuterium-exchanged APTES@SBA-15 and labeled as CO_2/D-APTES@SBA-15. The comparison of ^{1}H−^{13}C HETCOR spectra of CO_2/APTES@SBA-15 (Figure 9a) and CO_2/D-APTES@SBA-15 (Figure 9b) shows only regions of the spectra with signals corresponding to chemisorbed CO_2 species. Noticeably, upon deuterium exchange the cross-peaks corresponding to the ^{1}H resonances at $\delta_H \approx 4.2$, 4.4, and 4.8 ppm correlated with the ^{13}C peaks at 164, 160, and 153 ppm, respectively, vanish. On the contrary, the cross-peaks of all three ^{13}C resonances are correlated with the same ^{1}H resonance at $\delta_H \approx 2.9$ ppm in both, original and deuterated, samples. The same seems to happen for the resonance at $\delta_H \approx 1.8$ ppm. Based on experimental data, we can

DOI: 10.1021/jacs.6b11081
J. Am. Chem. Soc. 2017, 139, 389−408

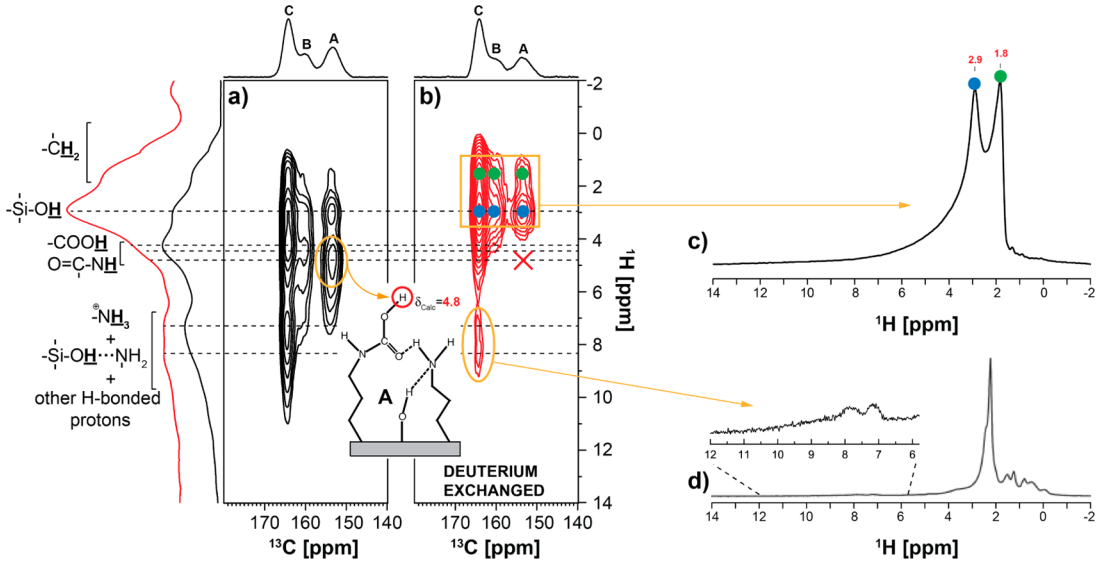

Figure 9. $^{1}H-^{13}C$ LG-CP HETCOR NMR spectra of (a) CO_2/APTES@SBA-15 and (b) CO_2/D-APTES@SBA-15 recorded at 16.4 T using a CT(LG-CT) = 2 ms. ^{1}H MAS NMR spectrum of parent SBA-15 (c) and ^{1}H Hahn-echo NMR spectrum CO_2/APTES@SBA-15 (d). Additional parameters provided in experimental section.

derive several explanations to aid in the assignment of the resonances, which are listed below:

(i) As discussed previously, the ^{13}C species **A** is extremely water-sensitive, thus suggesting that this specific chemisorbed CO_2 species is easily accessible since it vanishes in the presence of very low amounts of water. Thus, the amine yielding this chemisorbed CO_2 species is expected to be also easily accessible by H_2O/D_2O; its labile protons from the NH group are expected to exchange upon deuteration. Therefore, the question is what are the cross-peaks observed in the $^{1}H-^{13}C$ HETCOR spectrum after deuterium exchange (Figure 9b)? Obviously, they might be due to nonexchangeable or nonaccessible protons. The latter scenario is excluded, at least for the amines that lead to the formation of the species **A**, because this site is easily accessible by water as mentioned previously. The ^{1}H resonance at $\delta_H \approx 2.9$ ppm (and also at $\delta_H \approx 1.8$ ppm) is correlated to all chemisorbed CO_2 species whether the sample is deuterated or not. Since the amines giving rise to species **A** are fully accessible to D_2O, this cross-peak can only be ascribed to Si−OH protons that have not exchanged with deuterons as suggested in the literature.[77−79] In fact, a ^{1}H resonance at $\delta_H \approx 1.8$ and 2.9 ppm also appears in the ^{1}H MAS NMR spectrum of pure SBA-15 prior to amine functionalization (Figure 9c or S10), which supports its assignment to silanol groups. The $N-CH_2$ methylene protons from the alkyl chain are also visible between 1 and 2 ppm as they are the closest to the C═O carbon in all formed CO_2 species and do not exchange with deuterium as expected.

(ii) In the nondeuterated sample, chemisorbed CO_2 species produce cross-peaks with ^{1}H resonances at $\delta_H \approx 4.2$, 4.4, and 4.8 ppm. However, upon deuteration these signals disappear (Figure 9b). As these protons all resonate at similar frequencies and they all disappear upon deuteration, this could indicate that all these proton environments are associated with the same functional groups in species **A**, **B**, and **C**. The only exchangeable protons must come from non-hydrogen-bonded ND and COOD groups, which form upon deuteration followed by $^{13}CO_2$ adsorption, e.g., in −NHCOOH (neutral), $-^{+}NH_2COO^{-}$ (zwitterion), or $-NHCOO^{-}\cdots{}^{+}NH_2-C-$ (alkylammonium carbamate ion pair). Other environments are not chemically viable. Figure 9 provides additional proof that such acidic protons are not involved in strong HBs. Quantum mechanical calculations (discussed in section 3.4) support this conclusion; namely, calculated values of ^{1}H CSs appear between $\delta_H \approx 3.3-4.5$ ppm and are therefore in good agreement with our experiments.

(iii) Analyzing the proton projections of the 2D $^{1}H-^{13}C$ HETCOR NMR spectra of CO_2/APTES@SBA-15 (Figure 9, black line) and CO_2/D-APTES@SBA-15 (Figure 9, red line) we notice in the latter that the intensity of the broad ^{1}H resonance centered at $\delta_H \approx 7.3$ ppm have dramatically decreased when compared to the ^{1}H resonances at $\delta_H < 6$ ppm. This is the result of H/D exchange of protons mainly associated with the broad resonance (7.3 ppm). Conversely, signals at lower CSs correspond mostly to the population of inaccessible silanol groups (from inside the SBA-15 walls as shown by others[77−79]) and alkyl chain protons, which are harder to exchange. However, two faint ^{1}H resonances that have resisted the 24 h H/D exchange procedure are still visible at $\delta_H \approx 7.1$ and 8.2 ppm thus indicating that these ^{1}H peaks might be due to strong interactions involving species **C** (Figure 9b,d). In fact, this CS region is typical for hydrogen-bonded protons and their assignment will be further addressed in section 3.4. It is well known that protons engaged in strong HBs are not as easily exchanged as those that are interacting weakly.[80] That is a good reason why labile protons might have resisted deuterium exchange.

3.3.5.3. Detecting Interactions of Chemisorbed CO_2 Species with Silanols. 2D $^{1}H-^{29}Si$ HETCOR NMR spectrum of CO_2/APTES@SBA-15 (Figure 10a) was recorded to reveal which proton sites are closer to the identified T^n and Q^n silicon

DOI: 10.1021/jacs.6b11081
J. Am. Chem. Soc. 2017, 139, 389−408

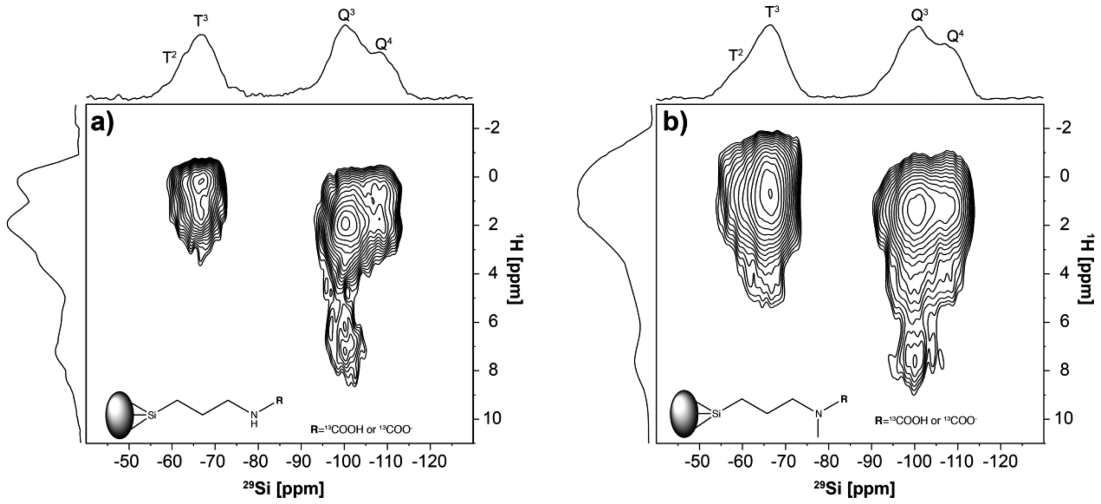

Figure 10. $^{1}H-^{29}Si$ CP HETCOR NMR spectra of (a) CO_2/APTES@SBA-15 and (b) CO_2/TMMAP@SBA-15 recorded at 9.4 T using contact time of 2 ms. Additional parameters provided in experimental section.

sites (n being the number of Si atoms at the second coordination sphere of a central Si atom). The spectrum shows that T^3 ($RSi(OSi)_3$) silicon species at $\delta_{Si} \approx -67$ ppm ("R" being the alkyl chain) are correlated to one main ^{1}H chemical environment at $\delta_H \approx 0.7$ ppm, which is associated with the $-Si(T^3)-CH_2-$ methylene protons. The signal at CSs associated with T^2 environments is not significant indicating that functionalizations occurred mainly in a tridentate mode. Q^3 ($Si(OSi)_3(OH)$) sites at $\delta_{Si} \approx -101$ ppm are correlated with ^{1}H CSs between 1 and 3 ppm, which were also observed in the ^{1}H MAS NMR spectrum of as-prepared SBA-15 at $\delta_H \approx 1.8$ and 2.9 ppm (Figure S10); Q^3 sites may also correlate with methylene protons from the alkyl chain, which appear in the same CS range as confirmed by the ^{1}H MAS NMR spectrum of amine-modified SBA-15 (Figure S9). Additional cross peaks are also observed between Q^3 site protons resonating at higher CS values (between 6 and 8 ppm). These ^{1}H resonances may correspond to surface silanols hydrogen-bonded to the amine group (Si−OH···N) according to molecular modeling (see section 3.4). Q^4 ($Si(OSi)_4$)) sites appearing at $\delta_{Si} \approx -109$ ppm show strong correlation mainly with the proton resonance centered at $\delta_H \approx 1$ ppm, corresponding to the $-$ Si-CH_2- group.

The $^{1}H-^{29}Si$ HETCOR NMR spectrum of degassed APTES@SBA-15 (Figure S12) and CO_2/APTES@SBA-15 (Figure 10a) exhibit similar features. While the spectrum of the former shows two extra cross-peaks correlating T^3 silicon species with protons centered at $\delta_H \approx 5$ ppm and $\delta_H \approx 7.5$ ppm, these cross peaks are only weakly observed in the latter spectrum. Nevertheless, calculations indicate (section 3.4 and Figure S20) that both these ^{1}H resonances correspond to the silanol protons interacting with carbamic acid/carbamate groups, i.e., protons hydrogen-bonded via either oxygen of the carbamic acid (δ_H(exp) ≈ 5 ppm vs δ_H(calc) ≈ 4.2 ppm) or the nitrogen of the amine group (δ_H(exp) ≈ 7.5 ppm vs δ_H(calc) ≈ 9−9.5 ppm). Such high-frequency resonances in the range between 7 and 8 ppm are also visible in the ^{1}H Hahn-echo NMR spectra of all amine-grafted SBA-15 materials prior to CO_2 adsorption (Figure S13). It is worth mentioning that such ^{1}H resonances have very low intensities (as only a few silanol groups remain after amine functionalization) and are not observed in the parent SBA-15 material (Figures S9 and S12), thus strongly supporting the idea that these protons must involve the presence of amines in HB with "very dilute" silanols.

As discussed before, we observed a ^{1}H CS at $\delta_H \approx 11.8$ ppm in the $^{1}H-^{13}C$ HETCOR NMR spectrum of CO_2/TMMAP@SBA-15 (Figure 8) and CO_2/N-3@SBA-15, which does not appear in the spectrum of CO_2/APTES@SBA-15 (Figure 7). The $^{1}H-^{29}Si$ HETCOR NMR spectrum of CO_2/TMMAP@SBA-15 (Figure 10b) was therefore acquired to ascertain if this high-frequency ^{1}H CS may or may not be ascribed to hydrogen-bonded Si−OH groups from the SBA-15 surface. This spectrum exhibits essentially the same features as the ones observed in the spectrum of CO_2/APTES@SBA-15 (Figure 10a). The highly deshielded proton at $\delta_H \approx 11.8$ ppm was not detected, which could raise doubts regarding what the exact nature of this proton species is. Fortunately, the absence of this cross-peak in the $^{1}H-^{29}Si$ HETCOR NMR spectrum should not be surprising as there are few reasons that could explain this. First, the high-frequency protons are associated with the species **B**, which presents just a small fraction of the overall chemisorbed CO_2 species formed. Also, the species are ^{13}C labeled, which greatly increases the sensitivity of ^{13}C NMR experiments compared to ^{29}Si ones. Second, the resonance at $\delta_H \approx 11.8$ ppm is assigned to non-silanol protons (see section 3.4), i.e., N-COOH protons in HB with neighboring amines. In this case, Si sites could be located too far from such protons. This would result in the weakening or quenching of possible internuclear H···Si dipolar couplings therefore precluding efficient CP transfer.

All this considered, the $^{1}H-^{29}Si$ HETCOR NMR spectra seem to clearly indicate that the Q^3 silanols are engaged in HBs with the grafted organic moieties. This is proven by the presence of an intense cross-peak centered at $\delta_H \approx 7.5$ ppm. Faint cross-peaks were also observed in the $^{1}H-^{13}C$ HETCOR NMR spectrum upon H/D exchange (Figure 9), around the same ^{1}H CS value, corresponding to dilute HB silanol species, thus sustaining our assignment.

3.4. Molecular Modeling of Amine···Chemisorbed CO_2 Species.

3.4.1. Optimization Approach for Cluster Models of Grafted Propylamines. Most of the silica materials studied in the literature that are functionalized with propylamine display high densities (above 1 molecule nm^{-2}) of propylamine chains on their surface. In the context of CO_2 adsorption, this is an

DOI: 10.1021/jacs.6b11081
J. Am. Chem. Soc. 2017, 139, 389−408

obvious approach to increase the number of sites that could interact with the gas molecules and, thus, increase the adsorption capacity and selectivity. With such high densities, it is expected that an interaction between neighboring amines can occur at the surface. To start our computational study, we have first considered small cluster systems where two propylamine chains are grafted to the silica surface at the smallest possible distance (0.57 nm; Figure 1), where all silicon alkoxide groups reacted with the surface. The amine density of these models are about 2.7 molecules/nm^2, which is comparable (only slightly above) to the values observed in the experimental samples of APTES@SBA-15 and TMMAP@SBA-15 (Table 1). This is a simplification of what may be the real chemical environment; second we also considered the effect of varying the distance between neighboring propylamine chains.

3.4.1.1. Optimization of Models Containing Amine···Amine HBs. To explore the possible structures of the propylamine chains on the silica surface model, several different starting structures were used in the optimization runs that converged to slightly different minima on the potential energy surface. The most stable structure is shown in Figure 1a. Several other similar but less stable structures were obtained after geometry optimization (e.g., Figure S14), when starting from different initial structures. In all cases, the amine moieties were engaged in a variety of different HB configurations. Nonlinear HB arrangement between amines (Figure S14a) and HB to oxygen atoms of the organosilica (Figure S14b) correspond to an energy increase of 12 and 2.5 kJ mol^{-1}, respectively, in relation to the minimum energy structure depicted in Figure 1a.

3.4.1.2. Optimization of Models Containing Amine···Amine and Amine···Silanol HBs. Nonreacted silanol groups are expected to exist at the pore surface, as the grafting procedure does not guarantee that all silanols react with the alkoxylsilanes. Therefore, the possible existence of propylamine groups interacting with silanols must be taken into account in the design of our models since a significant number of silanols were detected in the NMR experiments. Thus, clusters with the presence of two amines and at least one silanol were also considered here. The lowest energy structure found (Figure 1b) presents an HB between the silanol and one amine, and an additional HB between that amine and the neighboring amine group. These two concerted HBs are responsible for a significant stabilization of the structure (−48 kJ·mol^{-1}) when compared to other optimized structures with amines involved in a single HB (cf. Figure S15). Silanol groups were, therefore, included in the study of the properties of propylamine functionalized silicas, as they present strong interactions with the amine groups that can influence the structure of species formed with CO_2.

3.4.1.3. Optimizing Distances among Neighboring Amines: Comparing Calculated vs Experimental Amine Surface Densities. To assess the impact of this amine···amine distance on the existence of HBs between amines, the energy of molecular systems composed of two neighboring amines grafted on silica was monitored as a function of the distance between the two Si atoms at the base of the aminopropyl chains (Figures S16). The lowest energy value obtained corresponds to a distance between the two chains of 0.95 nm and was used as reference for calculating the energy differences. For Si−Si distances above 1.15 nm, the effect of the HB completely disappears. The results from Figure S16 can be used to estimate the density of amine groups on the silica surface that is required for the occurrence of HBs between amines by assuming the corresponding surface of a circle centered on the base of the aminopropyl chain with diameter 0.95 nm. Accordingly, surface densities above 1.41 molecules·nm^{-2} correspond to the situation where neighboring amines are most probably forming HBs (distances below 0.95 nm). In contrast, for surface densities below 0.96 molecules·nm^{-2}, most of the amine groups will not be able to form HBs with neighboring amines (distances above 1.15 nm). For intermediate densities (distances of 1.05 nm, i.e., about 1.15 molecules nm^{-2}), weak HB may be formed. The formation of HBs between amines on the surface is expected to influence the CO_2 capture efficiency, since several works have reported a decrease in the amine capturing efficiency with low densities of amine surface groups.[10,20,81,82] In fact, Danon et al.[20] reported that propylamine groups do not capture CO_2 when they are not forming HBs either with the neighboring amines or with silanol groups. The APTES densities in that case were below 0.66 molecules·nm^{-2}. Knowles et al.[82] concluded that for propylamine surface densities below ∼1 molecules·nm^{-2}, both the amount and the enthalpy for CO_2 adsorption are not significantly influenced by the amine concentration. Although the distribution of APTES on the porous silica materials may not be completely homogeneous, the values for amine surface density reported in the literature seem to agree with the threshold value (0.96 molecules·nm^{-2}) calculated for the existence of HBs between neighboring amines. In our present work, the APTES@SBA-15 material presented an average propylamine density of 2.37 molecules·nm^{-2} (Table 1) and strong interaction with CO_2, in line with the results reported in the literature. This density is clearly above the minimum density threshold estimated for the existence of HBs (1.41 molecules·nm^{-2}). In the models considered in our work (see below), we have assumed the case where the propylamine pairs can interact and, therefore, are bonded with the silica surface at the minimum energy inter-amine distance, i.e., amines densities ≥1.41 molecules·nm^{-2}. This situation is in fact the most common one in the experimental works reported in the literature, since it corresponds to the maximization of the amine grafting and CO_2 adsorption capacity. In the case of TMMAP@SBA-15 the amine surface density is very similar to that found for APTES@SBA-15 (Table 1) and is thus also above the minimum value calculated for the propylamine.

3.4.2. Correlating APTES/TMMAP···CO_2 Cluster Models with NMR Data. The structure of several APTES···CO_2 cluster models comprising one amine, one carbamic acid and one silanol group were optimized with their calculated ^{13}C NMR CS displayed in Figure S17 (without silanols), Figure S18 (with silanols) and for the most stable cases in Figure 12. As it can be seen, there are important differences between the ^{13}C CS calculated for different configurations of CO_2 interacting with APTES; in fact, in the case of chemisorbed CO_2 species, the ^{13}C CSs of the carbonyl are in the range from 160.9 to 163.7 ppm when the carbamic acid proton is involved in hydrogen bonding (Figures S17e and S18b−d,f), whereas the analogous carbons resonate in the range from 154.0 to 154.6 ppm when the carbamic acid proton is not hydrogen-bonded (Figures S17d and S18e,g). In the case of the physisorbed CO_2 species, the ^{13}C CS is similar to that of the gaseous CO_2 molecule. Additional detailed discussion about the energy of cluster models and calculated CS of carbonyl is presented in the SI. Calculations were also performed imposing a propylammonium carbamate ion pair geometry (Figure 11). Three structure

DOI: 10.1021/jacs.6b11081
J. Am. Chem. Soc. 2017, 139, 389−408

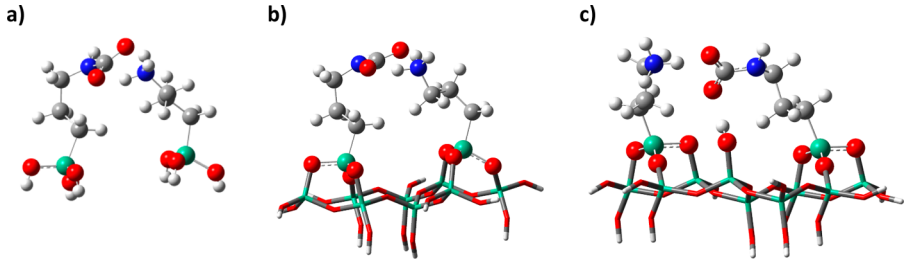

Figure 11. Structures of propylammonium carbamate ion pairs obtained by imposing three hydrogen atoms fixed at 1.0275 Å from one of the amine nitrogen atoms. a) without the presence of a silica surface, b) with the presence of silica surface, c) with the presence of a surface OH group forming an HB to the carbamate group.

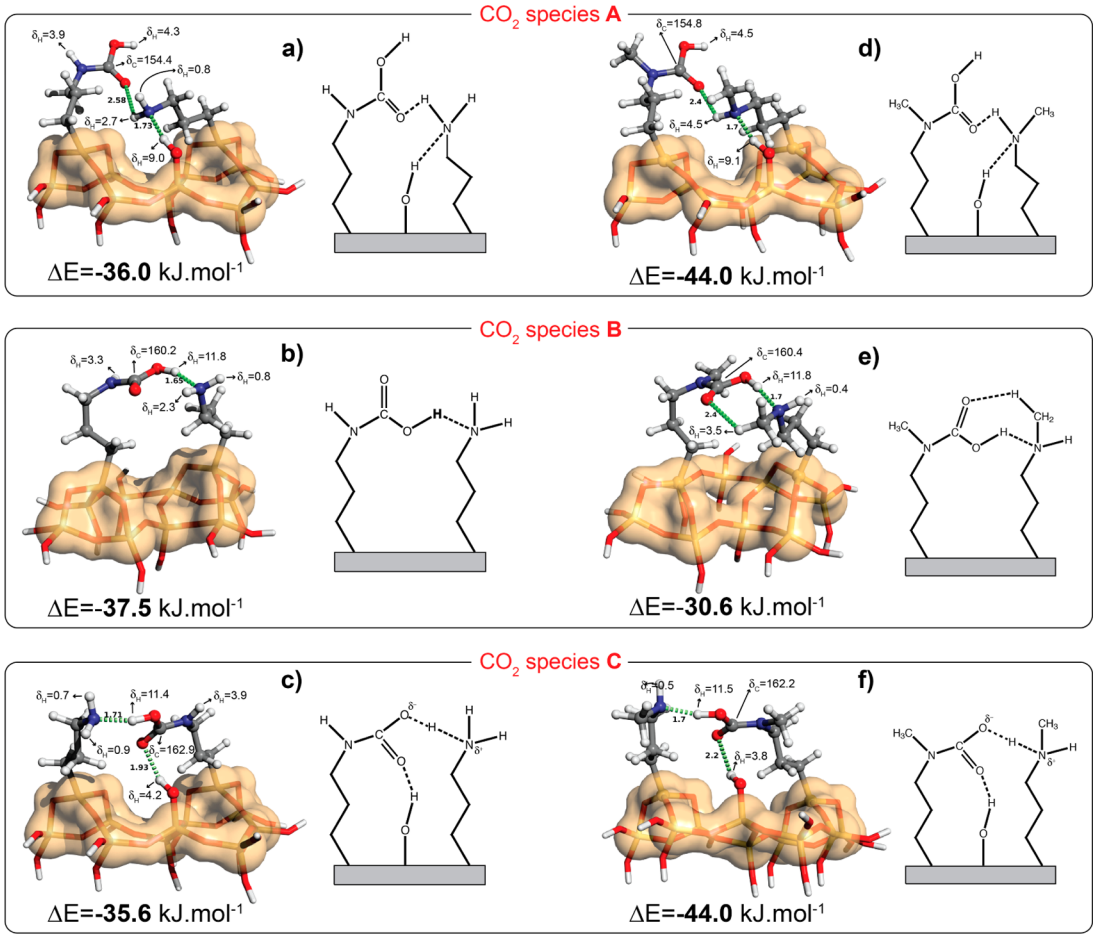

Figure 12. Most stable optimized structures representing species **A**, **B**, and **C** featuring one carbamic acid residue (from reaction of amines with CO_2) interacting with APTES (a–c) or TMMAP (d–f). In panels a, c, d, and f, the organic linkers are involved in hydrogen bonds with silanol groups from the silica surface, while panels b and e depict the situation where silanols are not interacting with the linkers. The stabilization energies (ΔE) are also shown. The relevant calculated ^{1}H and ^{13}C CSs (in ppm) are indicated in the figure along with the hydrogen bond distances (green dashed lines; values in Å) between distinct functional groups. See text for additional explanations.

models of propylammonium carbamate ion pairs were optimized with and without the presence of silica surface (Figure 11), enforcing three hydrogen atoms at a fixed distance (1.0275 Å, taken as the mean value for the N–H bonds in the fully optimized gas-phase propylammonium ion) from one nitrogen atom along with a neighbor deprotonated carbamate group. The calculated ^{13}C CSs of the structures with the imposed propylammonium carbamate ion pair, ranging from 168.5 to 170.8 ppm, are ~4–7 ppm higher than the most deshielded species **C** (~164 ppm) observed in the experimental ^{13}C spectrum. Nevertheless, the shift toward higher CS seems to support that **C** resonance is compatible with a very stable RNCOOH···NH_2R species (further discussion below). Notice however that the structures with the imposed propylammonium carbamate ion pair are ~50 kJ·mol^{-1} less stable than the corresponding structures with the neutral pairs having strong HBs (see topological discussion in SI). Therefore, when the three protons of the ammonium group (Figure 11) are allowed to relax, one of them is transferred to the carbamate species leading to structures as those displayed in Figure 12 a-c. This result agrees with the calculated CO_2 binding mechanism on an alkylamine functionalized MOF, where zwitterionic and

DOI: 10.1021/jacs.6b11081
J. Am. Chem. Soc. 2017, 139, 389–408

charged species were only obtained as intermediates to attain carbamic acid stabilized by HB.[83] Models with TMMAP were also optimized and calculated ^{13}C CS (Figure S19) are similar to those obtained for the APTES models (Figure S18).

^{13}C CPMAS NMR spectra of CO_2/APTES@SBA-15 (Figure 2) exhibit a ^{13}C resonance at $\delta_C \approx 153$ ppm (**A**) in all studied materials, which is in very good agreement with the calculated values for structures where the carbamic acid proton is not involved in HBs. The most stable structures containing APTES and TMMAP are depicted in Figure 12 with additional details (all calculated ^1H and ^{13}C CSs depicted in relevant models are shown in Figure S20 and Figure S21). The CS of the non-hydrogen-bonded carbamic acid (-N-COOH) proton (Figure 12a) is $\delta_H = 4.3$ ppm and is thus significantly lower than the ^1H CSs of hydrogen-bonded carbamic acid for which values of $\delta_H = 11.4$ ppm and $\delta_H = 11.8$ ppm were obtained (Figure 12 b and c). Non-hydrogen-bonded carbamic acid (Figure 12 a) with calculated CSs of $\delta_C = 154.4$ ppm and $\delta_H = 4.3$ ppm can also be matched with the experimentally observed NMR signals; namely, $^1H-^{13}C$ HETCOR NMR spectrum of the CO_2/APTES@SBA-15 exhibits a clear cross-peak correlating the ^{13}C resonance **A** at $\delta_C \approx 153$ ppm to the ^1H resonance at $\delta_H \approx 4.8$ (Figure 7). It is worth mentioning that calculations of the structure in Figure 12a with the presence of a water molecule in the vicinity of the carbamic acid proton yielded a final optimized structure with an HB engaged with the water oxygen (N-COOH···OH_2), exhibiting a $\delta_{calc}(^{13}C) = 161.0$ ppm (cf. Figure S18i) overlapping the resonances **B** and **C**. This provides an explanation to the behavior observed experimentally, i.e., the disappearance of species **A** upon hydration, and also brings more confidence to the accuracy of the computational approach employed here. All this considered, we believe the non-hydrogen-bonded carbamic acid complex represented in Figure 12a likely corresponds to the experimentally observed species **A**. The $^1H-^{13}C$ HETCOR NMR spectra (Figure 7) show a considerable diversity of ^1H chemical environments between 2 and 5 ppm, which coincide with calculated ^1H CS of NHC═O [$\delta_{calc}(^1H) = 3.3-3.9$ ppm, Figure 12a–c], free N-COOH [$\delta_{calc}(^1H) = 4.3$ ppm, Figure 12a] and hydrogen-bonded Si−OH [$\delta_{calc}(^1H) = 4.2$ ppm, Figure 12c]. In section 3.3.5.2 we have shown direct evidence of fast exchangeable protons from H/D exchange experiments in the same ^1H CS region as these resonances. This suggests that these chemical environments can be assigned to labile protons typically associated with N-COOH, NH and Si−OH functional groups. Calculations also show that silanol protons involved in hydrogen bonding with the amine group (Si−OH···N, Figure 12a) resonate at $\delta_{calc}(^1H) = 9.0$ ppm, while the one bonded to the C═O group (Si−OH···O═C, Figure 12c) resonates at $\delta_{calc}(^1H) = 4.2$ ppm. However, it should be stated that some silanol protons present in the parent SBA-15 do not exchange with deuterons (Figure 9).

From the previous section, the $^1H-^{29}Si$ HETCOR NMR spectrum clearly shows a H···Si correlation between the Q^3 silanol site and a ^1H environment between 4 and 5 ppm, which is close to the theoretical value of $\delta_{calc}(^1H) = 4.2$ ppm (Si−OH···O═C, Figure 12c). We also reported an experimental ^1H CS between 7 and 8 ppm associated with Q^3 silanol environments involved in the formation of a stronger type of HB. Encouragingly, a value of $\delta_{calc}(^1H) = 9.0$ ppm was calculated for the largest ^1H CS present in hydrogen-bonded silanol groups (Si−OH···N, Figure 12a), which supports the assignments above.

In the $^1H-^{13}C$ HETCOR spectrum (Figure 7), only resonance **C** shows proximity to high-frequency protons; namely, there is a cross-peak correlating species **C** with a "broad" ^1H resonance centered at $\delta_H \approx 7.3$ ppm. This was above tentatively assigned to protonated amines from propylammonium carbamate ion pairs, but calculations indicate that species **C** is involved in three HBs (cf. topological analysis and Table S3). From previous studies,[27,84] we have shown that ^{15}N CPMAS NMR measurements on CO_2 adsorbed on APTES-functionalized porous materials show a ^{15}N peak at ca. −350 ppm also typical of amino acid zwitterions. This could indicate that the formation of charged amine species (e.g., propylammonium carbamate) in porous systems might be a possibility. However, neutral amines also have CS in this range, showing that experimental values at ca. −350 ppm might not be conclusive in the present case. It is well known that protonation of amines may lead to relatively small ^{15}N CS differences (up to 20 ppm), unless the positive charge is strongly localized or the nitrogen atoms are involved in a π-bonded system.[85] The experimental broad ^1H resonance, centered at $\delta_H \approx 7.3$ ppm, readily disappears upon H/D exchange or after applying a dipolar filter using DQMAS spectroscopy. ^1H DQMAS NMR spectra (Figure S9) shows that this particular ^1H environment might be involved in moderately fast chemical exchange, which may lead to resonance broadening. Exchanging protons are expected to suppress the efficient excitation of DQ coherences in a DQMAS experiment thus resulting in the strong attenuation of the ^1H peak centered at 7.3 ppm when compared to the single pulse excitation NMR spectrum (cf. Figure S9a,b or Figure S9c,d). It is worth mentioning that much fainter resonances, assigned to hydrogen-bonded silanols, emerged at this same CS region only after H/D exchange (Figure 9).

The structure depicted in Figure 12b predicts the formation of carbamic acid with $\delta_{calc}(^{13}C) \approx 160$ ppm, remarkably close to the experimental values associated with species **B**. However, absence of an experimental cross-peak correlating this carbon resonance (**B**) and protons from hydrogen-bonded NCOOH suggests that this proton may be highly mobile precluding its detection in the NMR spectra. Alternatively, the absence of such cross-peaks may indicate that this site could also be associated with chemisorbed CO_2 species in the carboxylate ($NCOO^-$) form. Surprisingly, resonance **B**, from the $^1H-^{13}C$ HETCOR NMR spectrum of CO_2/TMMAP@SBA-15 (secondary amine), exhibits now a correlation with the high-frequency ^1H resonance at $\delta_H \approx 11.8$ ppm (Figure 8) thus indicating that in materials functionalized with secondary amines, species **B** is most likely found in its protonated (neutral) N-COOH form engaged in very strong hydrogen bonding, which is supported by the values of the topological analysis presented in Table S3 suggesting the RNCOO<u>H</u>···NH_2R HB in species **B** to be stronger than in the case of the species **C**. Very recently, it was suggested that the presence of carbamic acid moieties are predominant in secondary amines,[26] which is in agreement with the fact that a high-frequency ^1H resonance ($\delta_H \approx 11.8$ ppm) is only observed when SBA-15 is modified with the amines TMMAP (Figure 8) or N-3 (Figure S11), both incorporating a "secondary" amine group. Analogously, we assume that species **B** in CO_2/APTES@SBA-15 is also in the form of carbamic acid (NCOOH) according to the calculated structure depicted in Figure 12b. In addition, carbamic acid species are known to be unstable upon vacuum and heating treatments. This explains

DOI: 10.1021/jacs.6b11081
J. Am. Chem. Soc. 2017, 139, 389–408

why the ^{13}C resonance associated with this species (**B**) is strongly attenuated after 5 min of vacuum (Figure 4).

Cluster models with grafted TMMAP exhibit HBs formed between the carbamic acid and the surface silanols or the neighboring amine, similarly to what was found with the APTES clusters. Again, the ^{13}C CS values obtained are highly dependent on the type of formed HB and are very close to those obtained for the primary (APTES) amine when the HB network is similar. A minor difference of the TMMAP to the APTES cases is related to the presence of a methyl group. When the methyl group of TMMAP blocks the formation of the HB of the carbamic acid to neighboring amines (Figure S19d), the configuration becomes less stable; the energy is 25 kJ·mol^{-1} more positive than that calculated for the structure in Figure S19c where a strong HB exists. However, the ^{13}C CS (154 ppm) is close to that obtained when the C═O···HN HB is allowed to form (154.8 ppm). Calculated ^{13}C and ^{1}H NMR CSs for the optimized TMMAP models tend to be very similar to the ones obtained in the APTES models (cf. Figures S20d–f and S21a–g). The similarities in ^{13}C and ^{1}H CSs are even higher when only the lowest-energy structures depicted in Figure 12 for the APTES (panels a–c) and TMMAP (panels d–f) cases, respectively, are compared. This is expected because the nature of the functional groups is similar.

Simulations with clusters containing the N-3 diamine yielded structures similar to those already discussed for APTES and TMMAP. However, a significantly different mode of CO_2 bonding involving just the two intramolecular amine groups may occur is worth presenting here (Figure S22). Again, calculations show that amines are prone to have HBs with the surface silanols and that the reaction with CO_2 leads to more stable structures. In such cases, chemisorption of CO_2 yields a carbamic acid, which forms an HB with the other free amine group of the same chain and results in carbonyl CS around 160 ppm (Figure S22b,c).

3.5. Calculated IR Bands of the Optimized Models.

While we did not measured IR spectra of our $^{13}CO_2$ adsorbed AFMS materials due to the reasons explained in the introduction, the same structural models considered for the calculation of NMR data were used to compute IR absorption bands. Comparing the calculated IR bands with the ones found in literature can be interesting for testing the quality of the models to represent the systems under study, especially in the case of APTES functionalized SBA-15 for which there are numerous studies in the literature with IR data and band assignments. A detailed discussion of the results of the quantum mechanical calculations of the IR bands is presented in the Supporting Information. Briefly, the results indicate that the experimental data can be explained in light of the models presented, considering the lowest-energy structures depicted in Figure 12 for species **A**, **B**, and **C**, with the calculated N-COOH stretching of 1544–1514 cm^{-1} falling in the 1560–1510 cm^{-1} range experimentally reported.[10,18−20,22] The experimental IR bands of the chemisorbed CO_2 species on APTES functionalized silicas in dry conditions have been reported by several authors;[10,14,18−20,22,23,86−88] however, the band assignments are not consistent and may differ among studies. The disparity of conclusions regarding IR band assignment has been identified as a significant drawback in the clarification of the formed species on these systems.[1,2] In fact, several bands calculated on clusters shown in Figure S18 have been assigned to other species, i.e., ammonium and carbamate ions (charged species). We recall that the lowest energy models we have considered in our work consist only of neutral entities (Figure S18). To be more specific, the band at around 1700 cm^{-1} reported in some studies[18−20,22] under dry conditions fits well with the values obtained for some of our clusters (Tables S4 and S5), thus suggesting that these systems may comprise carbamic acid, which is hydrogen-bonded with neighboring amines. The N-COOH stretching is a relatively strong band (Figures S23 and S24) and should be easy to identify experimentally. Several studies describe bands at around 1560–1510 cm^{-1}[10,18−20,22] that we think could be due to the N-COOH stretching in the carbamic acid although they have often been assigned to other vibrations. According to our calculations, no other vibration appears in this range (Tables S4 and S5). Very recent works presented detailed IR measurements that are generally in agreement with spectra reported previously, but in which some of the bands are assigned to the presence of carbamic acid species.[89,90]

4. CONCLUSIONS

The intermolecular interactions involving chemisorbed CO_2 species inside amine-modified mesoporous silicas were studied by the combination of SSNMR and computer modeling, which proved to be very useful to approach these complex systems. With that purpose in mind, aminosilanes having distinct steric hindrances were grafted into SBA-15 and characterized. Different amines were shown to form distinct HB networks upon CO_2 adsorption, which may explain the different affinity of the materials for CO_2. Adsorption of $^{13}CO_2$ followed by a detailed SSNMR study, at variable pressures, was essential to unveil the complexity of the system, since several chemisorbed CO_2 species are formed even when just one type of amine is present.

The atomic-level study outlined revealed the speciation of chemisorbed CO_2 in AFMS materials. Experimental SSNMR combined with quantum mechanical calculations of ^{1}H and ^{13}C CSs, pointed toward the formation of CO_2 adducts stabilized through different combinations of HBs involving neighboring amine molecules and/or silanol groups from the silica surface. This approach allowed to shed light on the nature of the intermolecular interactions involved in the formation of CO_2 adducts. In-depth analysis of SSNMR and computational data of $^{13}CO_2$-loaded materials confirmed that what has previously been considered as unstable chemisorbed CO_2 species (carbamic acid) are very likely to exist in different molecular arrangements and explained the observed fast reversibility of CO_2 adsorption with pressure (i.e., the carbamic acid species are only observed under certain special conditions).

To summarize the main information retrieved from SSNMR; three ^{13}C resonances, named **A**, **B**, and **C** (150–170 ppm ^{13}C region), are present, which indicates the existence of, at least, three chemisorbed CO_2 species (essentially carbamic acid and alkylammonium carbamate-like ion pairs) in amine-modified SBA-15 materials, CO_2/APTES@SBA-15 and CO_2/TMMAP@SBA-15, containing primary and secondary monoamines, respectively. An extensive ^{1}H-based 1D/2D SSNMR study was carried out in these $^{13}CO_2$ loaded materials; in both situations high-frequency ^{1}H CSs between 7 and 8 ppm were found only to correlate with ^{13}C resonance **C** as observed from ^{1}H–^{13}C HETCOR NMR experiments. Experimental data for species **C**, resonating at $\delta_C \approx 164$ ppm, indicate that the OH and the C═O of the carbonyl are engaged in strong HBs with a neighboring amine and a surface OH group, respectively. The model structure with a calculated ^{13}C CS of $\delta_C \approx 162.2$–162.9

DOI: 10.1021/jacs.6b11081
J. Am. Chem. Soc. 2017, 139, 389–408

ppm is in excellent agreement with these structural HBs to the neighboring groups. Both experimental and computational results point to a species **C** having the carbonyl group strongly bound by HB with a high polarization of the atoms involved in these bonds. Although ionic species (i.e., complete removal of the proton from the acid group forming an ion pair) could also explain the experimental data, calculations imposing the propylammonium carbamate ion pair revealed this configuration to be energetically unfavorable (50 kJ mol^{-1} higher than the neutral pair) and thus less likely to occur in the absence of water in the systems.

^{1}H MAS and H/D exchanged $^{1}H-^{13}C$ HETCOR NMR spectra confirmed that the ^{1}H CS region contains other overlapping "*faint*" resonances from CO_2 adducts engaged in hydrogen bonding with "*dilute*" silanol groups. Furthermore, the most deshielded ^{1}H CS observed was displayed at ca. 11.8 ppm, and is only present for alkylamines comprising a *secondary amine*; the $^{1}H-^{13}C$ HETCOR NMR spectra of the materials grafted with secondary amines showed that this proton environment was only correlated with ^{13}C resonance **B**. A ^{1}H CS > 10 ppm suggests that this carbon environment is associated with a species involved in very strong HB with adjacent amines. Calculations demonstrated that this ^{1}H CS was in very good agreement with an HB of the type $-RNCOO\underline{H}\cdots NH_2R$, while also describing accurately the observed ^{13}C CS of species **B** ($\delta_C \approx 160$ ppm). $^{13}C\{^{14}N\}$ recoupling experiments excluded the possibility of carbonate and bicarbonate formation in the absence of water. The species formed are unstable and, to a large extent, can be removed when high vacuum is applied on the CO_2 loaded materials at ambient temperature. Species **A**, resonating at $\delta_C \approx 153$ ppm, was found to be extremely water-sensitive and, according to our models, is the only structure containing carbamic acid with its OH group not involved in HBs; indeed, species **A** is only engaged in very weak HB interactions through its C═O oxygen atom. A preliminary ^{13}C NMR spectrum of CO_2/APTES@SBA-15 grafted with a low concentration of APTES revealed that a ^{13}C resonance at the same CS as species **A** (always the weakest resonance in our work), dominates the spectrum. This result is a strong indication that CSs about 153 ppm correspond to a situation where the OH of the carbamic acid is not involved in hydrogen bonding. Although, a comprehensive study with variable amine loadings using amine groups with distinct chemical hindrances was beyond the scope of this work, this preliminary result indicates the importance of the amine loading on the speciation of the species formed, that needs to be addressed in detail in future works.

The $^{1}H-^{29}Si$ HETCOR NMR experiment further confirmed that the Q^3 surface silanols were indeed involved in HB contacts with the grafted alkylamines. It is worth mentioning that the model structure that matches species **B** (resonating at $\delta_C \approx 160$ ppm) was obtained when clusters with only two amines and without silanols were optimized. A theoretical CS of $\delta_C \approx 160$ ppm was obtained for such species, regardless of which alkylamine was employed (APTES or TMMAP). Experimental data for species **B** indicate that only the OH of the carbonyl is engaged in strong HB with a neighboring amine, as in the case of species **C**. Both experimental and computational results point to highly polarized OH moieties of the carbonyl group in species **B** and **C**. Although theoretical and experimental results are not completely unambiguous in this respect, we can hypothesize that species **B** might be formed in a surface region without available silanols in its vicinity. Calculations of ^{1}H CSs have also revealed fundamental structural insight on the type of the HB network formed, in most situations, corroborating the experimental ^{1}H NMR values associated with the strong HBs discussed above.

■ ASSOCIATED CONTENT

Supporting Information

The Supporting Information is available free of charge on the ACS Publications website at DOI: 10.1021/jacs.6b11081.

TG-DSC of materials; adsorption isotherms of CO_2 and CH_4; optimized cluster models with amines not forming HBs; cluster model used to calculate maximum interaction distance for HB formation; optimized clusters of APTES with CO_2; ^{1}H MAS and ^{1}H DQ MAS NMR spectra of APTES@SBA-15; comparison of possible structures of APTES-functionalized silica with and without CO_2; optimized clusters of TMMAP with and without CO_2; comparison of ^{1}H and ^{13}C CSs of possible structure of TMMAP-functionalized silica with and without surface OH groups; optimized clusters with N-3 and CO_2; topological analysis of the HB network of species **A**, **B**, and **C** in APTES@SBA-15; detailed presentation and discussion of calculated ^{13}C CS and IR bands for the optimized APTES-functionalized silica clusters, including Figures S1−S24 and Tables S1−S5 (PDF)

■ AUTHOR INFORMATION

Corresponding Authors

*lmafra@ua.pt

*moises.pinto@tecnico.ulisboa.pt

ORCID

João Pires: 0000-0002-8374-558X

José R. B. Gomes: 0000-0001-5993-1385

Moisés L. Pinto: 0000-0003-3061-9632

Notes

The authors declare no competing financial interest.

■ ACKNOWLEDGMENTS

The work was financed by Fundação para a Ciência e a Tecnologia (FCT) through projects IF/00993/2012/CP0172/CT0013 and PTDC/QEQ-QAN/6373/2014. This work was developed in the scope of the Projects POCI-01-0145-FEDER-007679|UID/CTM/50011/2013 (CICECO), UID/MULTI/00612/2013 (CQB), UID/ECI/04028/2013 (CERENA), financed by national funds through the FCT/MEC and cofinanced by FEDER under the PT2020 Partnership Agreement. The authors are also grateful to Investigador FCT program and to the Portuguese NMR Network (RNRMN).

■ REFERENCES

(1) Choi, S.; Drese, J. H.; Jones, C. W. *ChemSusChem* **2009**, *2*, 796−854.

(2) Bollini, P.; Didas, S. A.; Jones, C. W. *J. Mater. Chem.* **2011**, *21*, 15100−15120.

(3) Hiyoshi, N.; Yogo, K.; Yashima, T. *Chem. Lett.* **2004**, *33*, 510−511.

(4) Xu, X.; Song, C.; Miller, B. G.; Scaroni, A. W. *Ind. Eng. Chem. Res.* **2005**, *44*, 8113−8119.

(5) Franchi, R. S.; Harlick, P. J. E.; Sayari, A. *Ind. Eng. Chem. Res.* **2005**, *44*, 8007−8013.

DOI: 10.1021/jacs.6b11081
J. Am. Chem. Soc. 2017, 139, 389−408

(6) Li, W.; Choi, S.; Drese, J. H.; Hornbostel, M.; Krishnan, G.; Eisenberger, P. M.; Jones, C. W. *ChemSusChem* **2010**, *3*, 899−903.
(7) Sayari, A.; Belmabkhout, Y. *J. Am. Chem. Soc.* **2010**, *132*, 6312−6314.
(8) Ebner, A. D.; Gray, M. L.; Chisholm, N. G.; Black, Q. T.; Mumford, D. D.; Nicholson, M. A.; Ritter, J. a. *Ind. Eng. Chem. Res.* **2011**, *50*, 5634−5641.
(9) Tan, Z. *Air Pollution and Greenhouse Gases*; Springer: Singapore, 2014.
(10) Hiyoshi, N.; Yogo, K.; Yashima, T. *Microporous Mesoporous Mater.* **2005**, *84*, 357−365.
(11) Didas, S. A.; Sakwa-Novak, M. A.; Foo, G. S.; Sievers, C.; Jones, C. W. *J. Phys. Chem. Lett.* **2014**, *5*, 4194−4200.
(12) Choi, S.; Drese, H.; Eisenberger, P. M.; Jones, C. W. *Environ. Sci. Technol.* **2011**, *45*, 2420−2427.
(13) Ma, X.; Wang, X.; Song, C. *J. Am. Chem. Soc.* **2009**, *131*, 5777−5783.
(14) Leal, O.; Bolívar, C.; Ovalles, C.; García, J. J.; Espidel, Y. *Inorg. Chim. Acta* **1995**, *240*, 183−189.
(15) Yong, Z.; Mata, V.; Rodrigues, A. E. *Sep. Purif. Technol.* **2002**, *26*, 195−205.
(16) Hedin, N.; Andersson, L.; Bergström, L.; Yan, J. *Appl. Energy* **2013**, *104*, 418−433.
(17) Chen, C.; Kim, J.; Ahn, W.-S. *Korean J. Chem. Eng.* **2014**, *31*, 1919−1934.
(18) Bacsik, Z.; Ahlsten, N.; Ziadi, A.; Zhao, G.; Garcia-Bennett, A. E.; Martín-Matute, B.; Hedin, N. *Langmuir* **2011**, *27*, 11118−11128.
(19) Bacsik, Z.; Atluri, R.; Garcia-Bennett, A. E.; Hedin, N. *Langmuir* **2010**, *26*, 10013−10024.
(20) Danon, A.; Stair, P. C.; Weitz, E. *J. Phys. Chem. C* **2011**, 11540−11549.
(21) Srikanth, C. S.; Chuang, S. S. C. *J. Phys. Chem. C* **2013**, *117*, 9196−9205.
(22) Knöfel, C.; Martin, C.; Hornebecq, V.; Llewellyn, P. L. *J. Phys. Chem. C* **2009**, *113*, 21726−21734.
(23) Chang, A. C. C.; Chuang, S. S. C.; Gray, M.; Soong, Y. *Energy Fuels* **2003**, *17*, 468−473.
(24) dos Santos, T. C.; Bourrelly, S.; Llewellyn, P. L.; Carneiro, J. W.; Ronconi, C. M. *Phys. Chem. Chem. Phys.* **2015**, *17*, 11095−11102.
(25) Bali, S.; Leisen, J.; Foo, G. S.; Sievers, C.; Jones, C. W. *ChemSusChem* **2014**, *7*, 3145−3156.
(26) Hahn, M. W.; Jelic, J.; Berger, E.; Reuter, K.; Jentys, A.; Lercher, J. A. *J. Phys. Chem. B* **2016**, *120*, 1988−1995.
(27) Pinto, M. L.; Mafra, L.; Guil, J. M.; Pires, J.; Rocha, J. *Chem. Mater.* **2011**, *23*, 1387−1395.
(28) Sayari, A.; Belmabkhout, Y.; Da'na, E. *Langmuir* **2012**, *28*, 4241−4247.
(29) Sayari, A.; Heydari-Gorji, A.; Yang, Y. *J. Am. Chem. Soc.* **2012**, *134*, 13834−13842.
(30) Zhu, Y.; Zhou, J.; Hu, J.; Liu, H. *Catal. Today* **2012**, *194*, 53−59.
(31) Builes, S.; Vega, L. F. *J. Phys. Chem. C* **2012**, *116*, 3017−3024.
(32) Hedin, N.; Chen, L.; Laaksonen, A. *Nanoscale* **2010**, *2*, 1819−1841.
(33) Brunelli, N. A.; Didas, S. A.; Venkatasubbaiah, K.; Jones, C. W. *J. Am. Chem. Soc.* **2012**, *134*, 13950−13953.
(34) Young, P. D.; Notestein, J. M. *ChemSusChem* **2011**, *4*, 1671−1678.
(35) Choi, M.; Kleitz, F.; Liu, D.; Lee, H. Y.; Ahn, W.-S.; Ryoo, R. *J. Am. Chem. Soc.* **2005**, *127*, 1924−1932.
(36) Rouquérol, F.; Rouquérol, J.; Sing, K. *Adsorption by powders and porous solids*; Academic Press: San Diego, 1999.
(37) Lukens, W. W.; Schmidt-Winkel, P.; Zhao, D.; Feng, J.; Stucky, G. D. *Langmuir* **1999**, *15*, 5403−5409.
(38) Pires, J.; Carvalho, A.; Pinto, M.; Rocha, J. *J. Porous Mater.* **2006**, *13*, 107−114.
(39) Antao, S. M.; Hassan, I.; Wang, J.; Lee, P. L.; Toby, B. H. *Can. Mineral.* **2008**, *46*, 1501−1509.
(40) Lopez, N.; Illas, F.; Pacchioni, G. *J. Am. Chem. Soc.* **1999**, *121*, 813−821.
(41) Gomes, J. R. B.; Cordeiro, M. N. D. S.; Jorge, M. *Geochim. Cosmochim. Acta* **2008**, *72*, 4421−4439.
(42) Gomes, J. R. B.; Illas, F.; Silvi, B. *Chem. Phys. Lett.* **2004**, *388*, 132−138.
(43) Zhao, Y.; Truhlar, D. G. *J. Phys. Chem. A* **2006**, *110*, 5121−5129.
(44) Zhao, Y.; Truhlar, D. G. *Theor. Chem. Acc.* **2008**, *120*, 215−241.
(45) Hariharan, P. C.; Pople, J. A. *Theor. Chim. Acta* **1973**, *28*, 213−222.
(46) Francl, M. M.; Pietro, W. J.; Hehre, W. J.; Binkley, J. S.; DeFrees, D. J.; Pople, J. A.; Gordon, M. S. *J. Chem. Phys.* **1982**, *77*, 3654−3665.
(47) Frisch, M. J.; Trucks, G. W.; Schlegel, H. B.; Scuseria, G. E.; Robb, M. A.; Cheeseman, J. R.; Scalmani, G.; Barone, V.; Mennucci, B.; Petersson, G. A.; Nakatsuji, H.; Caricato, M.; Li, X.; Hratchian, H. P.; Izmaylov, A. F.; Bloino, J.; Zheng, G.; Sonnenberg, J. L.; Hada, M.; Ehara, M.; Toyota, K.; Fukuda, R.; Hasegawa, J.; Ishida, M.; Nakajima, T.; Honda, Y.; Kitao, O.; Nakai, H.; Vreven, T.; Montgomery, J. A., Jr.; Peralta, J. E.; Ogliaro, F.; Bearpark, M.; Heyd, J. J.; Brothers, E.; Kudin, K. N.; Staroverov, V. N.; Kobayashi, R.; Normand, J.; Raghavachari, K.; Rendell, A.; Burant, J. C.; Iyengar, S. S.; Tomasi, J.; Cossi, M.; Rega, N.; Millam, N. J.; Klene, M.; Knox, J. E.; Cross, J. B.; Bakken, V.; Adamo, C.; Jaramillo, J.; Gomperts, R.; Stratmann, R. E.; Yazyev, O.; Austin, A. J.; Cammi, R.; Pomelli, C.; Ochterski, J. W.; Martin, R. L.; Morokuma, K.; Zakrzewski, V. G.; Voth, G. A.; Salvador, P.; Dannenberg, J. J.; Dapprich, S.; Daniels, A. D.; Farkas, Ö.; Foresman, J. B.; Ortiz, J. V.; Cioslowski, J.; Fox, D. J. *Gaussian 09*, Revision B.01; Gaussian, Inc.: Wallingford, CT, 2009.
(48) Valero, R.; Gomes, J. R. B.; Truhlar, D. G.; Illas, F. *J. Chem. Phys.* **2008**, *129*, 124710.
(49) Valero, R.; Gomes, J. R. B.; Truhlar, D. G.; Illas, F. *J. Chem. Phys.* **2010**, *132*, 104701.
(50) Toda, J.; Fischer, M.; Jorge, M.; Gomes, J. R. B. *Chem. Phys. Lett.* **2013**, *587*, 7−13.
(51) Pillai, R. S.; Jorge, M.; Gomes, J. R. B. *Microporous Mesoporous Mater.* **2014**, *190*, 38−45.
(52) Perdew, J. P.; Schmidt, K. *AIP Conf. Proc.* **2000**, *577*, 1−20.
(53) Willoughby, P. H.; Jansma, M. J.; Hoye, T. R. *Nat. Protoc.* **2014**, *9*, 643−660.
(54) Wolinski, K.; Hinton, J. F.; Pulay, P. *J. Am. Chem. Soc.* **1990**, *112*, 8251−8260.
(55) Lodewyk, M. W.; Siebert, M. R.; Tantillo, D. J. *Chem. Rev.* **2012**, *112*, 1839−1862.
(56) Maciel, G. E.; Traficante, D. D. *J. Am. Chem. Soc.* **1966**, *88*, 220−223.
(57) Hagen, R.; Roberts, J. D. *J. Am. Chem. Soc.* **1969**, *91*, 4504−4506.
(58) *Computational Chemistry Comparison and Benchmark DataBase*. NIST Standard Reference Database Number 101, Release 17b, 2015; http://cccbdb.nist.gov/.
(59) Schmidt-Rohr, K.; Mao, J.-D. *Chem. Phys. Lett.* **2002**, *359*, 403−411.
(60) Haw, J. F.; Nicholas, J. B.; Xu, T.; Beck, L. W.; Ferguson, D. B. *Acc. Chem. Res.* **1996**, *29*, 259−267.
(61) Blasco, T. *Chem. Soc. Rev.* **2010**, *39*, 4685−4702.
(62) Thommes, M.; Kaneko, K.; Neimark, A. V.; Olivier, J. P.; Rodriguez-Reinoso, F.; Rouquerol, J.; Sing, K. S. W. *Pure Appl. Chem.* **2015**, *87*, 1051−1069.
(63) Greegg, S. J.; Sing, K. S. W. *Adsorption, surface area and porosity*, 2nd ed.; Academic Press Inc.: London, 1982.
(64) Saini, V. K.; Andrade, M.; Pinto, M. L.; Carvalho, A. P.; Pires, J. *Sep. Purif. Technol.* **2010**, *75*, 366−376.
(65) Sanz-Pérez, E. S.; Arencibia, A.; Sanz, R.; Calleja, G. *RSC Adv.* **2015**, *5*, 103147−103154.
(66) Huang, H. Y.; Yang, R. T.; Chinn, D.; Munson, C. L. *Ind. Eng. Chem. Res.* **2003**, *42*, 2427−2433.
(67) Zeleňák, V.; Badaničová, M.; Halamová, D.; Čejka, J.; Zukal, a.; Murafa, N.; Goerigk, G. *Chem. Eng. J.* **2008**, *144*, 336−342.
(68) Wang, L.; Yang, R. T. *J. Phys. Chem. C* **2011**, *115*, 21264−21272.

DOI: 10.1021/jacs.6b11081
J. Am. Chem. Soc. 2017, 139, 389−408

(69) Borrego, T.; Andrade, M.; Pinto, M. L.; Silva, A. R.; Carvalho, A. P.; Rocha, J.; Freire, C.; Pires, J. *J. Colloid Interface Sci.* **2010**, *344*, 603−610.
(70) Khatri, R. a.; Chuang, S. S. C.; Soong, Y.; Gray, M. *Ind. Eng. Chem. Res.* **2005**, *44*, 3702−3708.
(71) Khatri, R. A.; Chuang, S. S. C.; Soong, Y.; Gray, M. *Energy Fuels* **2006**, *20*, 1514−1520.
(72) Schmidt-Rohr, K.; Mao, J. D.; Olk, D. C. *Proc. Natl. Acad. Sci. U. S. A.* **2004**, *101*, 6351−6354.
(73) van Rossum, B.-J.; Castellani, F.; Pauli, J.; Rehbein, K.; Hollander, J.; de Groot, H. J. M.; Oschkinat, H. *J. Biomol. NMR* **2003**, *25*, 217−223.
(74) Yamauchi, K.; Kuroki, S.; Fujii, K.; ANDO, I. *Chem. Phys. Lett.* **2000**, *324*, 435−439.
(75) Martins, I. C. B.; Sardo, M.; Santos, S. M.; Fernandes, A.; Antunes, A.; André, V.; Mafra, L.; Duarte, M. T. *Cryst. Growth Des.* **2016**, *16*, 154−166.
(76) Gellman, S. H.; Dado, G. P.; Liang, G. B.; Adams, B. R. *J. Am. Chem. Soc.* **1991**, *113*, 1164−1173.
(77) Chuang, I. S.; Kinney, D. R.; Maciel, G. E. *J. Am. Chem. Soc.* **1993**, *115*, 8695−8705.
(78) Scholten, A. B.; de Haan, J. W.; Claessens, H. A.; van de Ven, L. J. M.; Cramers, C. A. *Langmuir* **1996**, *12*, 4741−4747.
(79) García, N.; Benito, E.; Guzmán, J.; Tiemblo, P.; Morales, V.; García, R. A. *Microporous Mesoporous Mater.* **2007**, *106*, 129−139.
(80) Englander, S. W.; Mayne, L. *Annu. Rev. Biophys. Biomol. Struct.* **1992**, *21*, 243−265.
(81) Zelenak, V.; Halamova, D.; Gaberova, L.; Bloch, E.; Llewellyn, P. *Microporous Mesoporous Mater.* **2008**, *116*, 358−364.
(82) Knowles, G. P.; Graham, J. V.; Delaney, S. W.; Chaffee, A. L. *Fuel Process. Technol.* **2005**, *86*, 1435−1448.
(83) Planas, N.; Dzubak, A. L.; Poloni, R.; Lin, L.-C.; McManus, A.; McDonald, T. M.; Neaton, J. B.; Long, J. R.; Smit, B.; Gagliardi, L. *J. Am. Chem. Soc.* **2013**, *135*, 7402−7405.
(84) Lourenço, M. A. O.; Siquet, C.; Sardo, M.; Mafra, L.; Pires, J.; Jorge, M.; Pinto, M. L.; Ferreira, P.; Gomes, J. R. B. *J. Phys. Chem. C* **2016**, *120*, 3863−3875.
(85) Mason, J. *eMagRes.* **2007**, 0343.
(86) Zheng, F.; Tran, D. N.; Busche, B. J.; Fryxell, G. E.; Addleman, R. S.; Zemanian, T. S.; Aardahl, C. L. *Ind. Eng. Chem. Res.* **2005**, *44*, 3099−3105.
(87) Srivastava, R.; Srinivas, D.; Ratnasamy, P. *J. Catal.* **2005**, *233*, 1−15.
(88) Srivastava, R.; Srinivas, D.; Ratnasamy, P. *Microporous Mesoporous Mater.* **2006**, *90*, 314−326.
(89) Foo, G. S.; Lee, J. J.; Chen, C.-H.; Hayes, S. E.; Sievers, C.; Jones, C. W. *ChemSusChem* **2016**, DOI: 10.1002/cssc.201600809.
(90) Yu, J.; Chuang, S. S. C. *Energy Fuels* **2016**, *30*, 7579−7587.

DOI: 10.1021/jacs.6b11081
J. Am. Chem. Soc. 2017, 139, 389−408